Generic Stochastic Modeling of Vehicle-to-Vehicle Wireless Channels

Authors: Petros Karadimas and David Matolak

Department of Computer Science and Technology

University of Bedfordshire, UK

Email: Petros.Karadimas@beds.ac.uk

Department of Electrical Engineering

University of South Carolina, USA

Email: matolak@sc.edu

Keywords: Fading channels, stochastic channel modeling, vehicle-to-vehicle (V-V) communications, wide sense stationary uncorrelated scattering (WSSUS) channels.

ABSTRACT

We present a generic statistical characterization of the vehicle-to-vehicle (V-V) wireless channel by adopting a stochastic modeling approach. Our approach is based on the doubly underspread (DU) property of non-wide sense stationary uncorrelated scattering (non-WSSUS) wireless channels, with V-V channels pertaining to this category. DU channels exhibit explicit frequency and time intervals over which they are approximated as WSSUS. We call these intervals restricted time interval (RTI) and restricted bandwidth (RBW), and variations taking place inside them are characterized as small scale variations. Large scale variations take place outside RTI and RBW. In this paper, we focus on small scale variations, thus, our modeling finds its applicability within RTI and RBW. As practical V-V channels exhibit rapid temporal fluctuations due to the inherent mobility of transmitter (Tx), receiver (Rx) and surrounding scatterers (e.g., other vehicles), we analyze the relevant second order statistics characterizing temporal variability, namely, the a) temporal correlation function (CF) (or autocorrelation function (ACF)), b) power spectral density (PSD) (or Doppler spectrum), c) level crossing rate (LCR) and d) average fade duration (AFD). Our analysis considers three-dimensional (3-D) scattering at the Tx and Rx together with random scatterers' mobility. Illustrative examples demonstrate the usefulness and flexibility of our analysis, which is further validated by fitting the theoretical LCR to an empirical, obtained at a US interstate highway. We show that significant Doppler frequencies can arise due to scatterers' mobility exceeding the respective maximum and minimum values when considering only Tx and Rx mobility. Also scatterers' mobility causes more rapid temporal variations when it becomes more intense. The latter is also true when 3-D scattering at the Tx and/or Rx spreads over a greater range of angular sectors and becomes less directional.

I. INTRODUCTION

The number and type of wireless communications applications continues to grow. One application of great current interest is Intelligent Transportation Systems (ITS), and within this broad area is communications between vehicles, or vehicle-to-vehicle (V-V) communications [1]. In V-V communications, the idea is that vehicles form networks exchanging information directly between each other in an ad-hoc manner. Thus, a wide range of safety, convenience and entertainment services can be

supported, such as emergency braking, notifications of hazards, notifications of traffic congestion, internet access for information and entertainment, etc. Information delivery requires a message from a source vehicle to propagate reliably in high-speed and on-road environments and this imposes a great challenge in designing robust V-V communication systems. This facilitates the necessity of accurate, and on the same time, generic V-V channel characterization.

For any wireless communication system, the channel is typically "uncontrolled" by the system designer and user. It is well known that the channel plays a critical role in communication reliability, and for V-V communications the channel will often be distorting, lossy, and rapidly time-varying. All these characteristics make it challenging for system designers to ensure reliable and timely communication. Hence, models for these channels represent vital tools for system developers [2**]**. These channels are the focus of this paper.

Currently planned V-V applications are expected to be short range, with link distances from a few meters to a kilometre. The three traditional channel effects that are used to characterize terrestrial wireless channels are propagation path loss (attenuation), large scale shadowing (or, obstruction), and small-scale (multipath) fading. These characteristics have been the focus of much analysis and many measurement campaigns, and research is currently ongoing.

The V-V channel can be very dynamic, with time variation rates up to double those of conventional cellular radio channels. For typical vehicles, V-V antenna heights will be low relative to other land mobile radio systems, and this will yield more frequent obstruction of the radio line of sight (LOS) between transmitter (Tx) and receiver (Rx). These effects can cause the V-V channel to yield more rapid and more severe fading than cellular channels. In light of the rapid time variation, the V-V channel is often best modelled as statistically non-stationary.

This paper describes characteristics of the physical wireless channel for V-V communication applications. In the remaining parts of this Introduction we first define the V-V channel and some common settings. We then describe some initial V-V communication technologies, followed by a brief summary of the unique features of the V-V channel. In Section II, we describe the state of the art in V-V channel modeling, and Section III provides a discussion of the V-V reference stochastic model. In Section IV, we present a second-order statistical characterization of small scale fading together with some illustrative examples. In Section V, we validate our

modeling approach by fitting the theoretical LCR to an empirical obtained at a US interstate highway [16] and in Section VI, we draw the conclusion.

A. The V-V Channel

The V-V channel is the wireless channel between two terrestrial vehicles, such as two automobiles, trucks, vans, buses, etc. Initial V-V communications will take place on established roads in cities, suburbs, highways etc. We do not consider "off-road" settings in this paper. Such "off-road" areas, e.g., forest or mountainous regions, will exhibit differences in the form of greater attenuation and obstruction. The channel may include a line-of-sight (LOS) path between Tx and Rx, or it may be an obstructed, or non-LOS (NLOS) link. Either or both vehicles may be in motion.

Fig. 1 illustrates an urban V-V scenario, in which the numbered lines indicate conceptual radio propagation paths. One Tx and one Rx are indicated; in general all vehicles will have both Tx and Rx. In suburban areas, the density of vehicles would generally be smaller, with buildings set farther back from the street. On expressways, vehicle density is time-dependent, especially near urban areas that see morning and evening "rush hours." Vehicle density will affect the V-V channel characteristics.

B. Initial V-V Systems

Although V-V communication could conceivably operate in any frequency band from VHF through SHF, spectrum is scarce and regulatory constraints yield limits to specific bands. The primary spectral band currently planned for V-V applications is the 5.9 GHz band, which has been allocated in the US and Europe. This band is cited in the Dedicated Short Range Communication (DSRC) standard [3], originated by the US Dept. of Transportation, but moved to the IEEE under the 802.11p group [4]. The standard is also known as Wireless Access for Vehicular Environments (WAVE) [5].

The DSRC band is from 5.85-5.925 GHz. It was originally divided into seven, 10-MHz channels, one of which is reserved for priority messages. Channels of width 20 MHz are also possible. The DSRC/802.11p standard is a modified version of the IEEE 802.11 wireless local area network (WLAN) standard. As such, modifications for higher mobility had to be developed. The standard specifies the the physical (PHY) and the medium access control (MAC) layer requirements. The modulation/multiplexing is orthogonal frequency division multiplexing (OFDM) with several modulation orders. Multi-access is via time division.

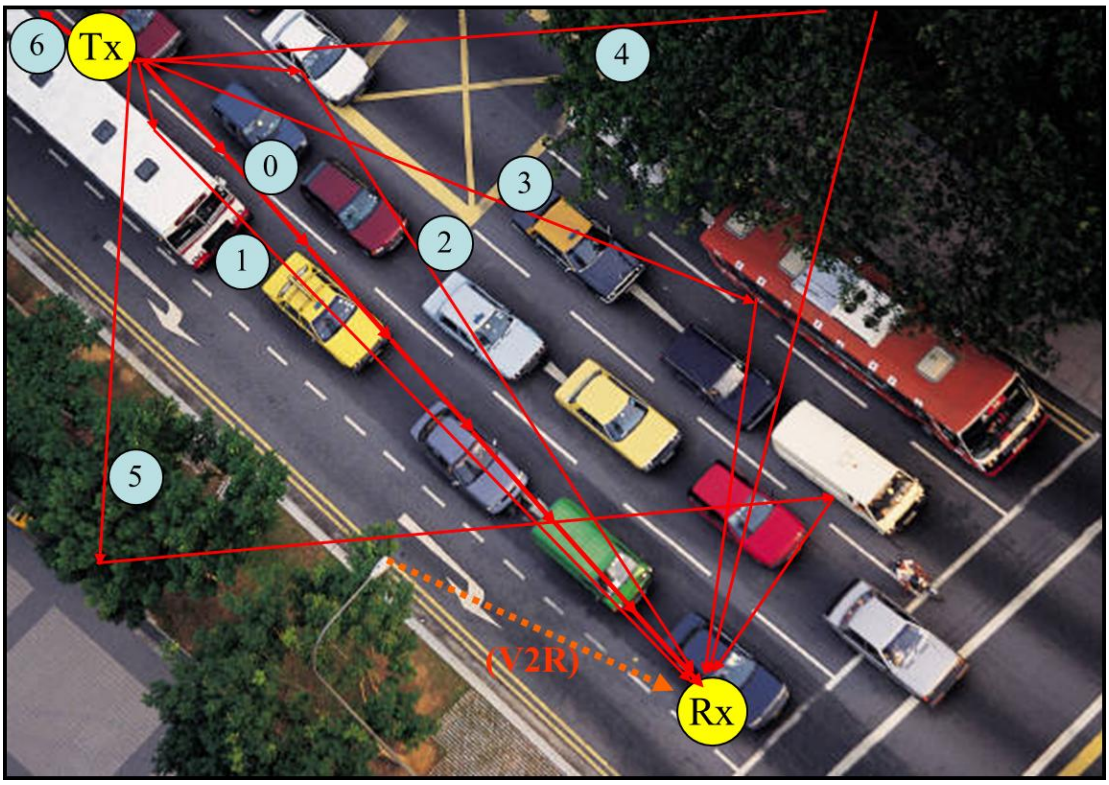

Fig. 1. Conceptual V-V channel between transmitter (Tx) and receiver (Rx) in urban area.

C. V-V vs. The Conventional Land Mobile Channel

Traditional land mobile radio channels have one end of the communication link fixed (non-mobile) at a so-called "base station" (BS). Such fixed stations typically have antennas atop tall towers, and access to ample electric power. The former characteristic will not apply in the V-V case where antenna heights will be only a few meters. Another physical feature distinct from traditional land mobile is that the V-V channel can have obstacles near/around both Tx and Rx, not just around the mobile unit.

In the V-V channel, obstacles to LOS propagation can be other vehicles, terrain, or buildings or other infrastructure (see Fig. 1). Link distances in urban areas are expected to be short, up to a few hundred meters or often much less. Link distances in suburban and expressway settings will often be larger (yet still less than the several kilometers of rural cellular). An additional unique feature of the V-V channel in comparison with cellular is that both Tx and Rx may be in motion. This can increase the rate of time variations in the V-V case to be double that of cellular. As noted, this more rapid time variation will often violate the conventional wide-sense stationarity (WSS) of the channel.

D. Channel Characterization Significance

As noted, regardless of the application or transmission technology, the wireless channel should be quantitatively characterized in order to optimize signaling design and performance [6]. Mathematical channel characterization results are typically employed in comparisons of competing technologies, and can aid design decisions on packet durations and format, channel bandwidths, etc. Models for the channel can also be used in analysis and computer simulations to estimate system performance, which in turn guides remedial measures (e.g., equalization, diversity) and system improvements.

Even with modern adaptive communication systems, channel impairments can severely degrade performance if not accounted for. Such performance degradations include a bit error probability "floor" or lower limit, and unacceptably large message latency. Long latencies can often be deemed link outages, which can sever multi-hop links. Thus, the V-V channel characteristics should be modelled as accurately as possible, since they affect system performance at multiple levels.

II. STATE OF THE ART

The wide sense stationary uncorrelated scattering (WSSUS) assumption holds generally with good accuracy in cellular communications, but not always in V-V communications. Thus, the statistical properties of V-V channels change with time (non-WSS) and frequency (non-US). This Section reviews the different modeling approaches used to characterize V-V channels, namely, a) deterministic (ray tracing) channel models, b) geometry-based stochastic channel models (GSCM) and c) stochastic channel models.

A. Deterministic models

This is a site-specific modeling approach providing realistic simulation of the wireless propagation environment [7]-[9]. It has the advantage of inherently incorporating the non-WSSUS property of V-V channels. For these models to be successful, accurate and detailed modeling of the propagation environment itself is required, and this can yield acceptable agreement between measured and simulated results [9]. These deterministic approaches employ ray-tracing (or ray-launching) to model the propagation environment constructed from a detailed database of all

obstacles and their electrical properties. However, very recently, other analytical methods such as the uniform theory of diffraction (UTD), the Poisson summation formula and the saddle point method have been employed to model vehicular communications in tunnels [10]. The inherent drawbacks of deterministic models are their high computational cost and restricted suitability for a specific propagation environment.

B. Geometry-based stochastic channel models (GSCM)

In this category, the transmitter, the receiver and the scatterers are parametrically located in space occupying certain positions in the propagation environment. There are two GSCM subcategories, namely, a) models where scatterers are located in rings and/or ellipses surrounding the Tx and/or the Rx, and b) models where scatterers are located in a more realistic way to better reproduce physical reality. The non-WSSUS property is not taken into account in the first subcategory, whereas it is inherently incorporated in the second.

In the first subcategory, reference [11] employed one circular ring of scatterers around the transmitter and one around the receiver, giving rise to double bouncing of multipath components along their way from the transmitter to receiver. A more generalized model was presented in [12], which combines a LOS component, single bouncing around the transmitter, single bouncing around the receiver and double bouncing at both sides. A more generalized model can be viewed in [13] with an additional elliptical ring of single bouncing scatterers surrounding the Tx and Rx. In [14], an algorithmic procedure was presented for determining the delay dependent power spectral density (PSD) with single bouncing scatterers uniformly distributed on an elliptical ring. The models in [11]-[14] considered two dimensional (2-D) multipath propagation. Three dimensional (3-D) multipath scattering was considered in [15] with similar double bouncing as in [11]. Extensions of [12] to account for 3-D scattering can be viewed in [16] and [17], with scatterers' mobility to be additionally incorporated in [18]. Extension of [13] to incorporate 3-D scattering can be viewed in [19].

In the second subcategory, scatterers are realistically (and randomly) located at the roadsides and between the road lanes in which the vehicles move [20]-[22]. The main propagation mechanisms that are realistically modelled are line-of-sight (LOS), discrete multipath components from mobile scatterers, discrete components from

static scatterers and diffuse components [20], [21]. In fact, such an approach is a street scattering modeling approach where each propagation mechanism is taken into account by simple statistical models for the surrounding objects. Propagation takes place in 2-D under a single bounce scattering regime.

C. Stochastic channel models

The models in this category provide the V-V channel statistics by employing the fewest number of parameters with the aim of maintaining simplicity and producing realistic solutions. A modern modeling approach considers that the channel statistics remain constant within certain time-frequency intervals [14]. In such intervals, which are also regarded as WSS intervals with respect to both time- and frequency-domains, the channel is characterized as doubly underspread and is modelled locally through the so called local scattering function (LSF) [23], [24]. The concept of LSF is an extension of the scattering function (SF) accounting for WSSUS channels [25].

By processing the LSF, V-V channel modeling has been pioneered by members of FTW in Austria and collaborators [26]-[29]. An important finding from [28] reports that for bandwidths that are intended to be used for V-V communications (i.e., 10 MHz), the channel will be WSS with respect to frequency (US assumption holds). In other words, the LSF is invariant with frequency provided that the time intervals have been selected such that the WSS assumption in the time-domain holds [26]. Another contribution of modeling WSS in time-domain through the LSF can be seen in [30].

Other contributions included the tapped-delay line (TDL) models as in [31] and [32] with different Doppler spectra for each tap and in [33] and [34] where the Weibull probability density function (PDF) was employed for the tap envelope fading distributions. Also, the authors in [33] model non-WSS with a “birth/death” process for generating taps. The authors in [34] extended the work in [33] to account for taps with correlated amplitudes and phases. A stochastic model based on measurements was presented in [35], where the Weibull PDF was used to model small scale fading variations and non-WSS was quantified through the correlation matrix distance metric [36]. Very recently, an interesting model was proposed in [37] accounting for a) vehicles’ location, b) first-order statistics (e.g., small scale fading, shadowing, received power) and c) performance evaluation in V-V channels. More specifically, vehicles’ location in space was modelled by a Cox spatial process, which in fact is an extension of a Poisson point process (PPP), which was used in [38] to model vehicles’

location. However, as was shown in [37], the PPP is suitable for modelling light traffic scenarios, while the Cox process can effectively model diverse traffic scenarios. In Cox spatial processes, the number of vehicles is generally modelled by Fox's-H PDFs, but for realistic V-V scenarios the negative binomial PDF was shown to be a proper model. Due to their high flexibility, Fox's-H PDFs were used to model small scale fading (they incorporate numerous small scale fading distributions), shadowing (as a substitute to lognormal), SNR and performance evaluation metrics such as symbol error probability (SEP) and channel capacity.

We report several other contributions on stochastic models, which mainly account for the temporal second-order statistics of V-V channels [39]-[47]. The most important are the a) temporal correlation function (CF) (or autocorrelation function (ACF)), b) power spectral density (PSD) (or Doppler spectrum), c) level crossing rate (LCR) and d) average fade duration (AFD). However, we should keep in mind that such modelling is only possible within the WSS intervals with respect to both time- and frequency-domains. In [39], the ACF and PSD were derived in the presence of 2-D isotropic scattering in both the transmitter and receiver sides, whereas [40] derived the LCR and AFD for the same scattering scenario. Extension of [39] can be seen in [41] when 3-D isotropic scattering occurs and extension of [40] in [42] under the presence of several 2-D anisotropic scattering scenarios. Extension of [41] can be seen in [43] regarding the ACF when 3-D anisotropic scattering occurs. In [44] and [45], the ACF, PSD, LCR and AFD were derived for a Hoyt V-V channel fading model under the presence of 2-D isotropic and anisotropic scattering, respectively. References [39]-[45] do not incorporate the realistic impact of other vehicles' mobility, with the latter being treated in [46] and [47]. However, [46] unrealistically considers fixed velocities for all mobile scatterers and [47] unrealistically considers totally random directions of movement of mobile scatterers (i.e., uniformly distributed)[1] and unrealistically equal amplitudes for all diffuse multipath components. Also [46] and [47] focus on analyzing ACF and PSD only and not LCR and AFD.

III. V-V CHANNEL MODEL DESCRIPTION

The V-V wireless channel is typically modeled by following a similar stochastic

[1] In V-V channels, mobile scatterers (i.e., other vehicles) will likely move in specific directions.

approach to that in [48, Ch. (1)]. Thus, if $x(t)$ is the transmitted signal in complex baseband form, the complex baseband form of the received signal $y(t)$ will be

$$y(t) = \sum_{l=1}^{L} a_l \exp(j2\pi v_l t) x(t - \tau_l) \tag{1}$$

where t is the time and L the total number of multipath components. The remaining parameters of the l^{th} multipath component are the complex amplitude a_l, i.e., $a_l = |a_l| \exp(j\phi_l)$ with ϕ_l the random phase, the delay τ_l, and the Doppler frequency v_l.

The reference model in equation (1) does not take into account dual antenna polarization, with such an extension being straightforward. In dual polarization modeling, four similar expressions to equation (1) are required to account for all possible combinations of co-polarized and cross-polarized transmitting-receiving antenna pairs. For the sake of simplicity, we consider single antenna polarization which captures all the important V-V channel characteristics presented here.

The rationale behind equation (1) is that the received signal consists of arbitrarily weighted, delayed and phase-shifted replicas of the transmitted signal, having the form $|a_l| \exp(j\phi_l) \exp(j2\pi v_{d,l} t) x(t - \tau_l)$. The Doppler frequency v_l arises because of the mobility of either or both the transmitter and receiver and the interaction of the l^{th} multipath component with mobile scatterers, e.g., vehicular traffic, wind-blown trees/vegetation and pedestrians. The delay τ_l results from the different path lengths that each multipath component travels from the transmitter along the way to the receiver. The complex amplitude a_l depends on the complex electric field of the l^{th} multipath component and also on the field patterns of the transmitting and receiving antennas.

The input-output relationship in equation (1) can be written in an equivalent integral form as follows[2]

$$y(t) = \int\int H(\tau, v) x(t - \tau) \exp(j2\pi v t) d\tau dv \tag{2}$$

[2]It is implied that the integral limits, when not given, cover the entire range of integration of the integrated variables. The same practice applies for the remainder of this paper.

where $H(\tau,v)$ is the delay-Doppler variant channel response defined as

$$H(\tau,v)=\sum_{l=1}^{L}a_l\delta(\tau-\tau_l)\delta(v-v_l) \tag{3}$$

with $\delta(.)$ being the Dirac delta function. Equation (2) can be written in a more compact form as follows

$$y(t)=\int h(\tau,t)x(t-\tau)d\tau \tag{4}$$

where $h(\tau,t)$ is the delay-time variant channel response (i.e., the impulse response) obtained by the inverse Fourier transform of $H(\tau,v)$ with respect to the Doppler frequency v. Thus,

$$h(\tau,t)=\int H(\tau,v)\exp(j2\pi vt)dv\,. \tag{5}$$

By further defining $x(t)$ with respect to its Fourier transform $X(f)$, i.e., $x(t)=\int X(f)\exp(j2\pi ft)df$, equation (4) can be written as

$$y(t)=\int G(f,t)X(f)\exp(j2\pi ft)df \tag{6}$$

where $G(f,t)$ is the frequency-time variant channel response (or the time-varying transfer function) obtained by the Fourier transform of $h(\tau,t)$ with respect to the delay τ. Thus,

$$G(f,t)=\int h(\tau,t)\exp(-j2\pi f\tau)d\tau=\int\int H(\tau,v)\exp(j2\pi vt)\exp(-j2\pi f\tau)d\tau dv\,. \tag{7}$$

Substituting equation (3) into equation (7) we have

$$G(f,t)=\sum_{l=1}^{L}|a_l|\exp(j\phi_l)\exp(j2\pi v_lt)\exp(-j2\pi f\tau_l)\,. \tag{8}$$

All channel responses in equations (3), (5) and (7) are equivalent representing variations in different domains and connected through Fourier transform relations [25]. Particularly, as can be seen from equation (7), $G(f,t)$ and $H(\tau,v)$ constitute a double Fourier transform pair. The received signal variations represented by equations (2) or (4) or (6) are characterized as small scale variations or small scale fading. These variations occur within "small" regions, i.e., regions with dimensions comparable with the size of the wavelength. Small scale fading modeling is essential to evaluate, validate and compare transmission standards serving as reference for simulations. However, as temporal variability and changing location are explicitly related [49, Ch. (2)], small scale fading can be limited to such frequency-time intervals where the V-V channel is approximated as WSSUS [23], [24], [48, Ch. (1)] or quasi-WSSUS [25]. In fact, such frequency-time intervals can be defined analogously to the definition of local area [49, Ch. (4)], as the maximum intervals in frequency and time over which the frequency-time variant channel response is written in the form of equation (8) having $\{|a_l|\}$, $\{\tau_l\}$ and $\{v_l\}$ constants. We call such intervals restricted time interval (RTI) (see also [50]) and restricted bandwidth (RBW). The phases $\{\phi_l\}$ are the random variables making $G(f,t)$ a random frequency-time varying complex process, i.e., a complex stochastic process[3]. Moreover, if $\{\phi_l\}$ are uncorrelated and uniformly distributed variables in $[-\pi,\pi]$, then, $G(f,t)$, will be a WSS process with respect to frequency and time[4]. Under the same conditions, the V-V channel is also first order stationary inside RTI and RBW[5]. Thus, small scale fading (variations within RTI and RBW) in V-V channels can be modelled by the well-established statistical tools for WSSUS channels as in [23] and [25].

Apart from small scale variations, V-V channels exhibit large scale variations, or large scale fading, arising from variations in the average received power (averaged about ten-forty wavelengths, see [51, Ch. (5)]) for fixed transmitter-receiver distance. Such variations take place in "large" regions on the order of hundreds of wavelengths and are attributed to shadowing by other obstacles (i.e., mainly other vehicles) occupying the path between the transmitter and the receiver. This type of fading is

[3] Frequency-time variations are clearly evident from equations (7) and (8) and also implied by equations (3) and (5) through their respective Fourier transform interrelations.

[4] A proof can be seen in [49, pp. (98-99)] for space-frequency varying channels written in the form of [49, eq. (4.4.1)]. A similar proof can be derived for frequency-time varying channels written in the form of equation (8). Alternatively, the impulse response is WSS with respect to time and US with respect to delay, i.e., WSSUS.

[5] A proof can be seen in [49, pp. (108-110)] for space-frequency varying channels written in the form of [49, eq. (4.4.1)]. A similar proof can be derived for frequency-time varying channels written in the form of equation (8).

also called shadow fading. Large scale fading modeling is essential for purposes such as link budget design and outage analysis. However, as reported in [23] and [48, Ch. (1)], shadowing is a major source of non-WSSUS behavior. Particularly, non-WSSUS behavior can be regarded as a large scale effect in the sense that mechanisms that generate non-WSSUS (e.g., shadowing, changes in the propagation environment, etc) vary much slower than small scale fading [23], [48, Ch. (1)]. With the existence of frequency-time intervals where the V-V channel is WSSUS (small scale fading intervals RTI and RBW), a new stochastic modeling approach is required to account for large scale variations incorporating non-WSSUS. Superimposed upon the small scale variations, a complete V-V channel characterization will then result. This approach is an open issue, however, a theoretical analysis in [50] demonstrated the validity of the Gaussian distribution to account for shadowing variability (in logarithmic scale) within different RTIs in fixed wireless channels but not for the V-V setting. The composite model in [37] combined small scale fading and shadowing, but it was focused on first-order statistical characterization only.

Finally, the V-V channel exhibits a deterministic variation arising from variations of the average received power with respect to the distance between the transmitter and receiver. The underlying effect is called path-loss and results in a monotonic decrease of average received power with respect to distance. The interested reader is referred to [52] for path-loss modeling in V-V channels.

IV. STATISTICAL CHARACTERIZATION

The frequency-time variant channel response $G(f,t)$ is an ensemble of several frequency-time realizations having the form of equation (8). Thus, statistical tools should be employed for characterizing the random nature of $G(f,t)$. The two universally accepted types of characterization are the first-and second-order statistical characterization. First-order statistical characterization arises when only one sample of $G(f,t)$ with respect to frequency and time is used to characterize channel behavior. Second-order statistical characterization uses two samples in frequency and/or time. One common assumption essential for both types of characterization is that of wide sense ergodicity [49, Ch. (5)]. Wide sense ergodicity means that all possible expected values of $G(f,t)$ with respect to one or two frequency-time samples can arise from only one frequency-time realization without considering the

whole ensemble of realizations. If this holds for all expected values with respect to any number of frequency-time samples (and not for only one or two), the process will be strict sense ergodic.

A. First order statistical characterization

First order characterization considers only one sample of the channel response with respect to frequency and time, thus $G(f,t)$ can be treated as complex random variable of the form

$$G = \sum_{l=1}^{L} |a_l| \exp(j\Phi_l) = g \exp(j\Phi) \tag{9}$$

where Φ_l sums all the phase terms in equation (8). A simple, yet physical, way to model the amplitude term is to group the terms $|a_l| \exp(j\Phi_l)$ in equation (9) into specular and diffuse components [49, Ch. (4)], [53], [54]. Specular components are a small number of strong multipath components and diffuse components are a large number of weak multipath components. Mechanisms such as LOS propagation and reflections from large smooth surfaces create specular components. Diffuse components are inherent to almost every wireless propagation channel and are attributed to different mechanisms such as scattering from rough surfaces and multiple bounces among different objects.

Thus, grouping the multipath components into specular and diffuse results in the following representation of equation (9) [49, Ch. (4)], [53], [54]

$$G = \sum_{l=1}^{L_s} |b_l| \exp(j\Phi_{s,l}) + \sum_{l=1}^{L_d} |c_l| \exp(j\Phi_{d,l}) = B \exp(j\Phi_s) + C \exp(j\Phi_d) \tag{10}$$

where L_s is the number of specular components (relatively small) and L_d is the number of diffuse components (large, i.e., $L_s << L_d$). The pairs b_l, $\Phi_{s,l}$, and c_l, $\Phi_{d,l}$, represent the amplitude and phase terms of the specular and diffuse components, respectively. In turn, B, Φ_s and C, Φ_d represent the total amplitude and phase of the specular and diffuse parts, respectively. First order statistical characterization

accounts for statistically modeling the amplitude of G. The phase terms in equations (9) and (10) are modeled as uniformly distributed random variables in $[-\pi, \pi]$.

The above grouping seems arbitrary, however some general principles apply. The rationale is to consider a small number of strong specular components and incorporate the remaining multipath components into the diffuse part of equation (10). Each diffuse component carries a small amount of multipath power and the total number of diffuse components gives rise to the so-called diffuse power which is much larger than the power of an individual diffuse component. A condition of the following form characterizes diffuse components and total diffuse power [49, eq. (4.3.3)]

$$\max(|c_l|^2) << \sum_{l=1}^{L_d} |c_l|^2 . \tag{11}$$

Thus, we can incorporate all the multipath components in the diffuse part of equation (10) and then exclude those components that do not satisfy condition (11). The process ends when condition (11) is satisfied by all the remaining components, whereas the excluded components will constitute the specular part.

The physical modeling approach of equation (10) generates several PDFs that can be appropriate for V-V channels. In the most general case treated in [54], amplitudes b_l are dependent positive random variables. The phases $\Phi_{s,l}$ are independent of b_l and also independent of each other and uniformly distributed in $[-\pi, \pi]$. The specular part will not obey the central limit theorem (CLT) and will be a complex non-Gaussian random variable. However, the CLT holds for the diffuse part because of the large number of multipath components.

The model in [54] generates several other PDFs encountered in the literature as special cases [49, Ch. (5)], [53], [55]. If there is no specular part, i.e., $L_s = 0$, only the diffuse part of equation (10) exists leading to a Rayleigh PDF [49, Ch. (5)]. The Rayleigh PDF is appropriate when multipath propagation occurs in dense scattering environments such as V-V channels under heavy traffic with obstructed LOS path [56]. The existence of one specular component, i.e., $L_s = 1$, with deterministic amplitude, b_1, together with the diffuse part of equation (10) leads to a Rice PDF [49, Ch. (5)]. The Rice PDF is suitable for V-V channels when the LOS path is

unobstructed [56]. Apart from the Rayleigh and Rice, the literature contains several other PDFs based on the general model of equation (10). More specifically, [55] contains the PDF for an arbitrary number of random specular components with statistically dependent amplitudes and no diffuse part, i.e., $L_d = 0$. Also, in [49, Ch. (5)] and [53], the two wave with diffuse power (TWDP) PDF was presented, i.e., the PDF that arises when two specular components with deterministic amplitudes together with diffuse part exist, i.e., $L_d >> 0$ and $L_s = 2$.

B. Second order statistical characterization

Second order characterization considers two samples of the channel response with respect to frequency and time. Of particular importance is the four-dimensional frequency-time-dependent correlation function (CF) $R(.,.;.,.)$ arising after taking the following expectation of $G(f,t)$ [23]

$$R(f,t;\Delta f,\Delta t) = E[G^*(f,t)\,\mathrm{G}(f+\Delta f, t+\Delta t)]. \tag{12}$$

The frequency-time-dependent scattering function (SF) $P(.,.;.,.)$, or the local scattering function (LSF), as is well-known [23], [24], is obtained by taking the double Fourier transform of $R(f,t;\Delta f,\Delta t)$ with respect to the frequency and time difference Δf and Δt, respectively. Thus [23]

$$P(f,t;\tau,v) = \int\int R(f,t;\Delta f,\Delta t)\exp(-j2\pi v\Delta t)\exp(j2\pi\tau\Delta f)\,d\Delta t\,d\Delta f\,. \tag{13}$$

As was shown in [23] and [24], a non-WSSUS channel can be locally approximated by a WSSUS, or a WSS with respect to both frequency and time. This approximation holds within the RTI and RBW, i.e., the stationarity region (see Fig. 2). Within the stationarity region, the assumption $P(f,t;\tau,v) \approx P(f_0,t_0;\tau,v) \approx P_S(\tau,v)$ holds (see [23] and [24]), where (f_0,t_0) is the centre of this region. Moreover, $P_S(\tau,v)$ is a nonnegative function of τ and v representing a SF and that is why the non-WSSUS V-V channel can be approximated by a WSSUS channel inside the stationarity region. In fact, this is an implication of the so-called doubly underspread (DU) property that practical wireless channels possess as demonstrated in [23]. In DU wireless channels,

there exists a much smaller coherence region inside the stationarity region (see Fig. 2) in which the transfer function is approximately constant, i.e., $G(f,t) \approx G(f_0,t_0)$. In the stationarity region, we also have from equation (13) $R(f,t;\Delta f,\Delta t) \approx R(f_0,t_0;\Delta f,\Delta t) \approx R_S(\Delta f,\Delta t)$. Thus, we obtain

$$P_S(\tau,v) = \int\int R_S(\Delta f,\Delta t)\exp(-j2\pi v\Delta t)\exp(j2\pi\tau\Delta f)d\Delta t d\Delta f \tag{14}$$

which is the well-known result relating the SF $P_S(\tau,v)$ and CF $R_S(\Delta f,\Delta t)$ in WSSUS channels as a double Fourier transform pair [25], i.e., $R_S(\Delta f,\Delta t) \overset{2F}{\longleftrightarrow} P_S(\tau,v)$, where $\overset{2F}{\longleftrightarrow}$ denotes the double Fourier transform pair.

Equation (14) offers a complete second-order statistical characterization of small scale fading (variations within RTI and RBW) in V-V channels from which several other metrics can arise. For example, the temporal CF, or the autocorrelation function (ACF) $R_{ST}(\Delta t)$, is $R_{ST}(\Delta t) = R_S(0,\Delta t)$. In turn, $R_{ST}(\Delta t)$ is a Fourier transform pair with the power spectral density (PSD), or Doppler spectrum $P_{SD}(v)$, i.e., $R_{ST}(\Delta t) \overset{F}{\longleftrightarrow} P_{SD}(v)$, defined as $P_{SD}(v) = \iint P_S(\tau,v)d\tau$. Thus, from equation (14)

$$P_{SD}(v) = \int R_{ST}(\Delta t)\exp(-j2\pi v\Delta t)d\Delta t. \tag{15}$$

In a similar way, we define the frequency CF $R_{SF}(\Delta f) = R_S(\Delta f,0)$ and power delay profile (PDP) $P_{ST}(\tau) = \iint P_S(\tau,v)dv$, being a Fourier transform pair, i.e., $R_{SF}(\Delta f) \overset{F}{\longleftrightarrow} P_{ST}(\tau)$. Thus, from equation (14)

$$P_{ST}(\tau) = \int R_{SF}(\Delta f)\exp(j2\pi\tau\Delta f)d\Delta f\ . \tag{16}$$

We now consider a narrowband (no frequency variations) V-V channel with 3-D scattering at both the Tx and Rx. The existence of mobile scatterers (e.g., other vehicles) between the Tx and Rx is also assumed. We aim at determining the second order statistics, namely, the ACF, PSD, LCR and AFD for characterizing the temporal variability of V-V channels within the stationarity region.

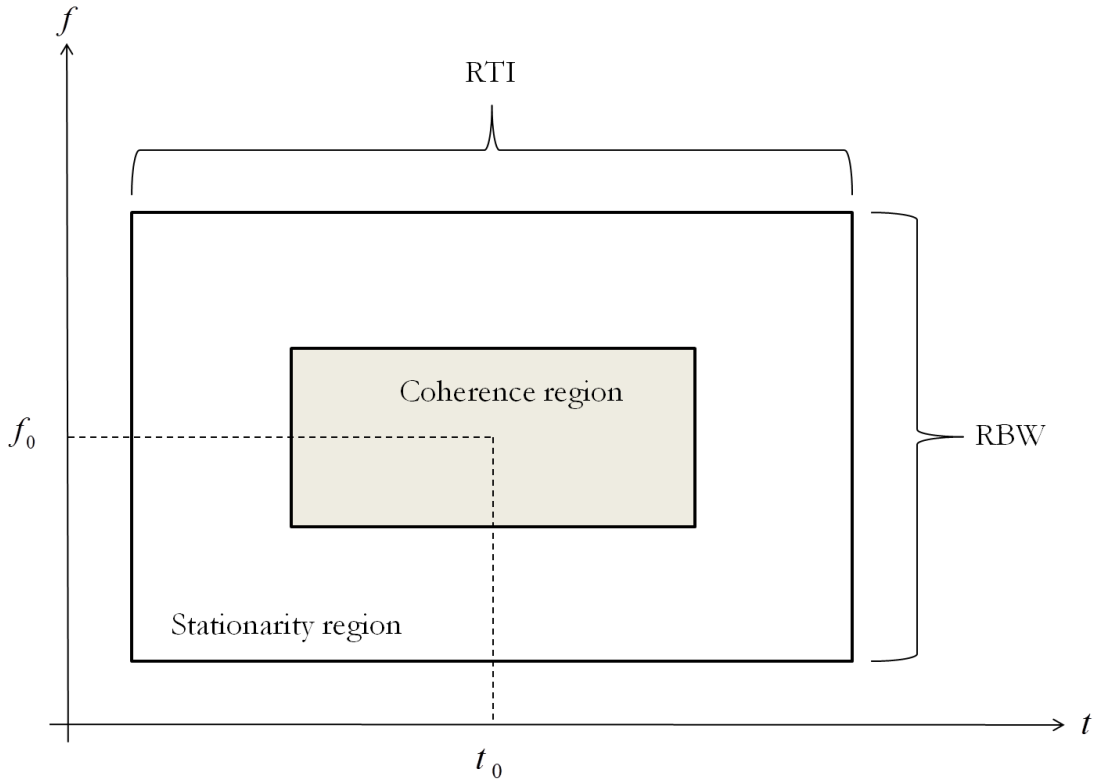

Fig. 2. Schematic representation of the coherence and stationarity regions in DU wireless channels.

The new form for equation (8) will be $G_N(t) = G(0,t)$. Thus

$$G_N(t) = \sum_{l=1}^{L} |a_l| \exp(j\phi_l) \exp(j2\pi v_l t). \tag{17}$$

The Doppler frequency v_l is determined by

$$v_l = v_{T,l} + v_{S,l} + v_{R,l} \tag{18}$$

where $v_{T,l}$, $v_{S,l}$ and $v_{R,l}$ are the contributions due to Tx mobility, scatterers' mobility and Rx mobility, respectively. The Doppler shift $v_{T(R),l}$ results from the departure (arrival) of the l^{th} multipath component from the mobile Tx (to the mobile Rx), as illustrated in Fig. 3. It is defined as [57]

$$v_{T(R),l} = v_{T(R)max} \cos\beta_{T(R),l} \cos\alpha_{T(R),l} \tag{19}$$

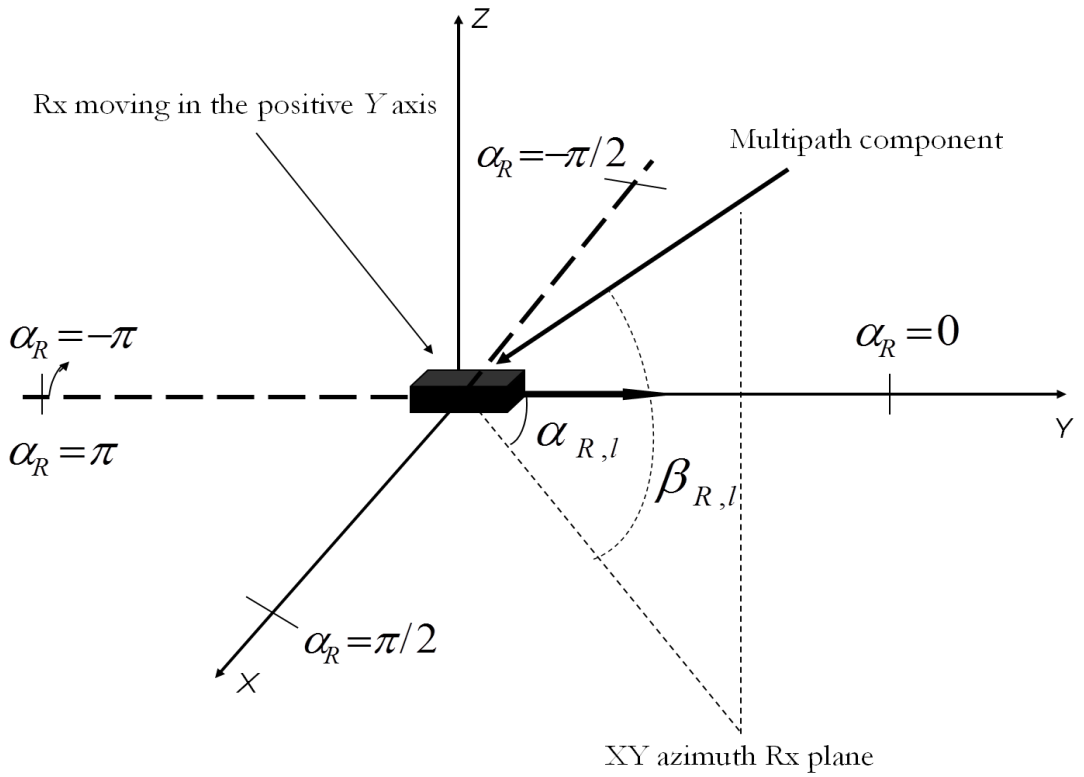

Fig. 3. 3-D arrival of a multipath component at the Rx side.

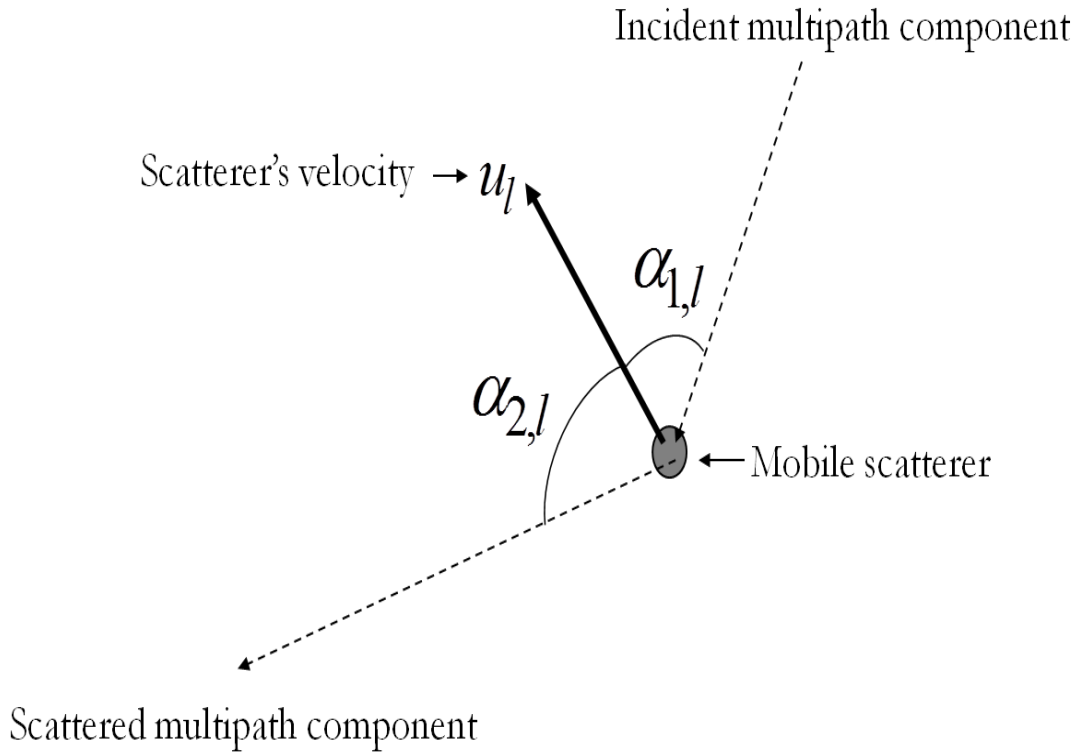

Fig. 4. Interaction of a multipath component with a mobile scatterer.

where $v_{T(R)max} = u_{T(R)} / \lambda$, λ is the carrier wavelength, $u_{T(R)}$ the Tx (Rx) velocity, $\alpha_{T(R),l}$ the azimuth angle of departure (AOD) (angle of arrival (AOA)) and $\beta_{T(R),l}$ the elevation AOD (AOA) with respect to the Tx (Rx) motion (see Fig. 3). $\alpha_{T(R),l}$ counts from the value $-\pi$ in the negative *Y* axis returning to the same point in the clockwise direction and $\beta_{T(R),l}$ is zero on the *X*-*Y* plane, $\pi/2$ on the positive *Z* axis and $-\pi/2$ on the negative *Z* axis. The Doppler shift $v_{S,l}$ results from the interaction of the l^{th} multipath with a single mobile scatterer, as illustrated in Fig. 4. Thus [58]

$$v_{S,l} = (u_{S,l} / \lambda)(cos\alpha_{1,l} + cos\alpha_{2,l}) \tag{20}$$

where $u_{S,l}$ is the scatterer's velocity, $\alpha_{1,l}$ the AOA and $\alpha_{2,l}$ the AOD with respect to scatterer's motion (see Fig. 4).

As an illustrative example for practical V-V channels, we consider that both the Tx and Rx move with maximum speeds $u_{Tmax} = u_{Rmax} = 30m/sec = 108km/hour$. We also assume that the maximum speed of mobile scaterrers is $u_{Smax} = 30m/sec$ (e.g., another vehicle). If the V-V communication system operates at $f_c = 6GHz$, the maximum Doppler shift will be $v_{max} = v_{Tmax} + v_{Rmax} + v_{Smax} = (f_c / c)(u_{Tmax} + u_{Rmax} + u_{Smax}) = 1800Hz$. Thus the minimum coherence in time is determined as $T_{cmin} = 1/v_{max} = 5.556 \cdot 10^{-4} sec$. Assuming the waves travel at most $d = 300m$, the maximum delays are $\tau_{max} = d/c = 10^{-6} sec$. Thus, the minimum coherence in frequency is $F_{cmin} = 1/\tau_{max} = 10^6 Hz$. This yields the size of the coherence region to be $T_{cmin}F_{cmin} = 555.6$. We next consider a maximum spatial extension and angular spread of mobile scatterers as $\omega_{max} = 10m$ and $\delta_{max} = \pi/30$, respectively. Then, the minimum stationarity in time, i.e., the RTI, can be determined as $T_{smin} = 1/\Delta v_{max} = 5.308 \cdot 10^{-3} sec$, where $\Delta v_{max} = 2v_{max} sin(\delta_{max}/2) = 188.409Hz$ [23]. Also the minimum stationarity in frequency, i.e., the RBW, can be determined as $F_{smin} = 1/\Delta\tau_{max} = 3 \cdot 10^7 Hz$, where $\Delta\tau_{max} = \omega_{max}/c = 0.333 \cdot 10^{-7} sec$ [23]. This yields the size of the stationarity region to be $T_{smin}F_{smin} = 159240 >> T_{cmin}F_{cmin} = 555.6$ giving

rise to the DU property of V-V channels. For this example, we see that each stationarity region contains approximately 286 coherence regions.

Now, assuming that the multipath power consists of one LOS component combined with diffuse power, the amplitude PDF, $p_{G_N}(.)$, of $G_N(t)$ will be Rician, which is suitable for V-V channels with unobstructed LOS path [56]. Thus [49, eq. (5.3.7)]

$$p_{G_N}(z) = z\exp[-(z^2+\rho^2)/(2\sigma^2)]I_0(z\rho/\sigma^2)/\sigma^2 \tag{21}$$

where $I_0(.)$ is the zero-order modified Bessel function [49, Appendix (A)], ρ is the amplitude of the LOS component and $2\sigma^2$ is the mean power of the diffuse part. Under the absence of LOS ($\rho = 0$), the Rayleigh PDF arises.

Using equation (17) in equation (12) and performing the expectation, we obtain with the aid of equations (18), (19) and (20), the ACF, $R_{SN}(\Delta t)$, as follows[6]

$$R_{SN}(\Delta t) = R_D(\Delta t) + \rho^2\exp(j2\pi v_{LOS}\Delta t) \tag{22}$$

where v_{LOS} is the deterministic Doppler shift of the LOS component. $R_D(\Delta t)$ represents the ACF due to the diffuse part, which arises by considering an infinite number of multipath components in equation (17) (a continuous version of equation (17)) making all discrete quantities in equations (19) and (20) to be represented by continuous random variables. Thus, after some manipulations

$$\begin{aligned} R_D(\Delta t) = 2\sigma^2 \int\int\int\int\int\int\int & exp(j2\pi v_{Tmax}\cos\beta_T\cos\alpha_T\Delta t)exp(j2\pi u_S\cos\alpha_1\Delta t/\lambda)\times \\ & exp(j2\pi u_S\cos\alpha_2\Delta t/\lambda)exp(j2\pi v_{Rmax}\cos\beta_R\cos\alpha_R\Delta t)\times \\ & p(\alpha_T,\beta_T,u_S,\alpha_1,\alpha_2,\alpha_R,\beta_R)d\alpha_T d\beta_T du_S, d\alpha_1, d\alpha_2, d\alpha_R, d\beta_R \end{aligned} \tag{23}$$

where $p(\alpha_T,\beta_T,u_S,\alpha_1,\alpha_2,\alpha_R,\beta_R)$ is the joint PDF of multipath power distributed over α_T, β_T, u_S, α_1, α_2, α_R, β_R.

[6] For uncorrelated and uniformly distributed in $[-\pi,\pi]$ phases $\{\phi_l\}$.

We consider the impact of scatterers' mobility to be decomposed from the impact of Tx and Rx mobility. Thus u_S, α_1, α_2 can be modelled independently from α_T, β_T, α_R, β_R. Naturally, α_1, α_2 and u_S can be also considered independent with respect to each other. We further assume that the AOD at the Tx can be decomposed from the AOA at the Rx. The latter gives rise to the so-called Kronecker model with separable spatial correlations at the Tx and Rx [59]. However, this assumption was questioned in publications that followed, see e.g., [60] and [61]. As a general trend, we state the less dependence between AOD and AOA comes together with the more diffusive nature of the channel [62]. Finally, we assume statistical independence between the azimuth and elevation AODs and AOAs. Such assumption can be valid only when multipath propagation results from a single cluster, or under specific assumptions for the azimuth and elevation AODs and AOAs in multi-clustered scenarios [63]. Based on the above assumptions, the joint PDF in equation (23) is decomposed to the product of the marginal PDFs, i.e., $p(\alpha_T,\beta_T,u_S,\alpha_1,\alpha_2,\alpha_R,\beta_R)=p_{\alpha_T}(\alpha_T)p_{\beta_T}(\beta_T)p_{u_S}(u_S)p_{\alpha_1}(\alpha_1)p_{\alpha_2}(\alpha_2)p_{\alpha_R}(\alpha_R)p_{\beta_R}(\beta_R)$, where, for example, $p_{\alpha_T}(\alpha_T)$ is the marginal PDF for the diffuse multipath power distributed over the azimuth AOD.

Under the aforementioned assumptions, equation (23) can be simplified as

$$R_D(\Delta t)=2\sigma^2 R_T(\Delta t)R_S(\Delta t)R_R(\Delta t) \tag{24}$$

where $R_{T(R)}(\Delta t)$ and $R_S(\Delta t)$ represent the ACFs due to a) scattering around the Tx (Rx) and b) scaterrers' mobility, respectively, defined as

$$R_{T(R)}(\Delta t)=\iint exp(j2\pi v_{T(R)max}\cos\beta_{T(R)}\cos\alpha_{T(R)}\Delta t)p_{\alpha_{T(R)}}(\alpha_{T(R)})p_{\beta_{T(R)}}(\beta_{T(R)})d\alpha_{T(R)}d\beta_{T(R)} \tag{25}$$

$$R_S(\Delta t)=\iiint exp(j2\pi u_S\cos\alpha_1\Delta t/\lambda)exp\left(j2\pi u_S\cos\alpha_2\Delta t/\lambda\right)\times$$
$$p_{u_S}(u_S)p_{\alpha_1}(\alpha_1)p_{\alpha_2}(\alpha_2)du_S d\alpha_1 d\alpha_2 \tag{26}$$

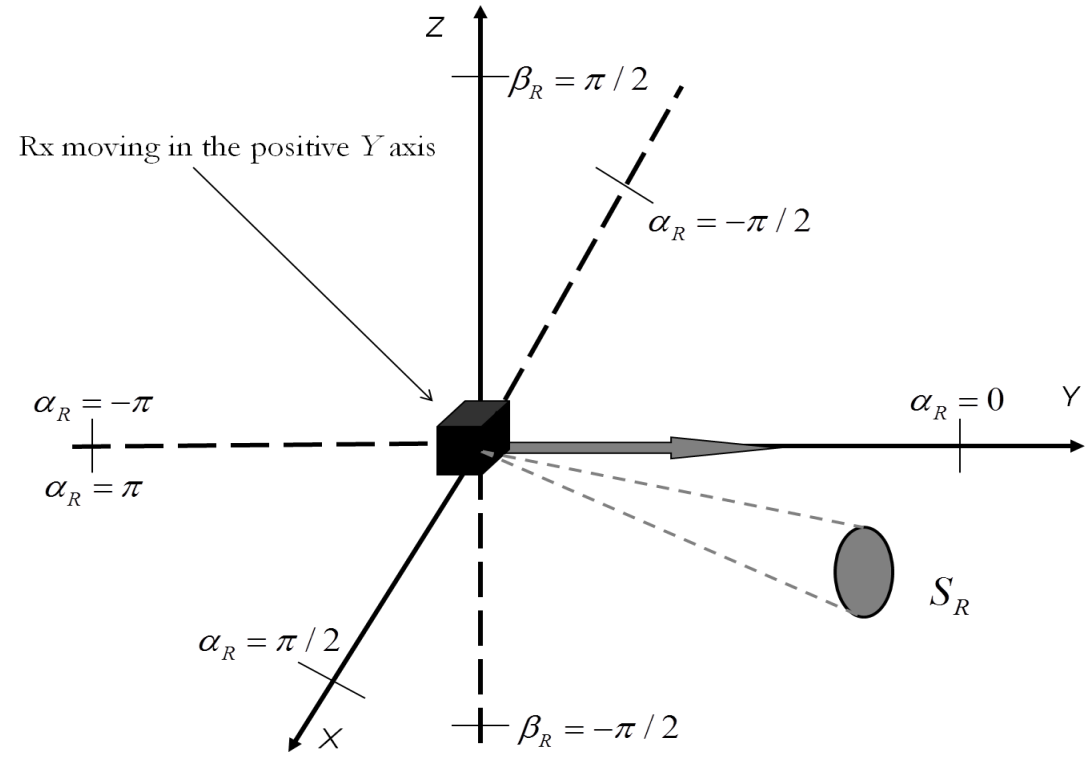

Fig. 5. A 3-D uniform sector of arrival at the Rx side.

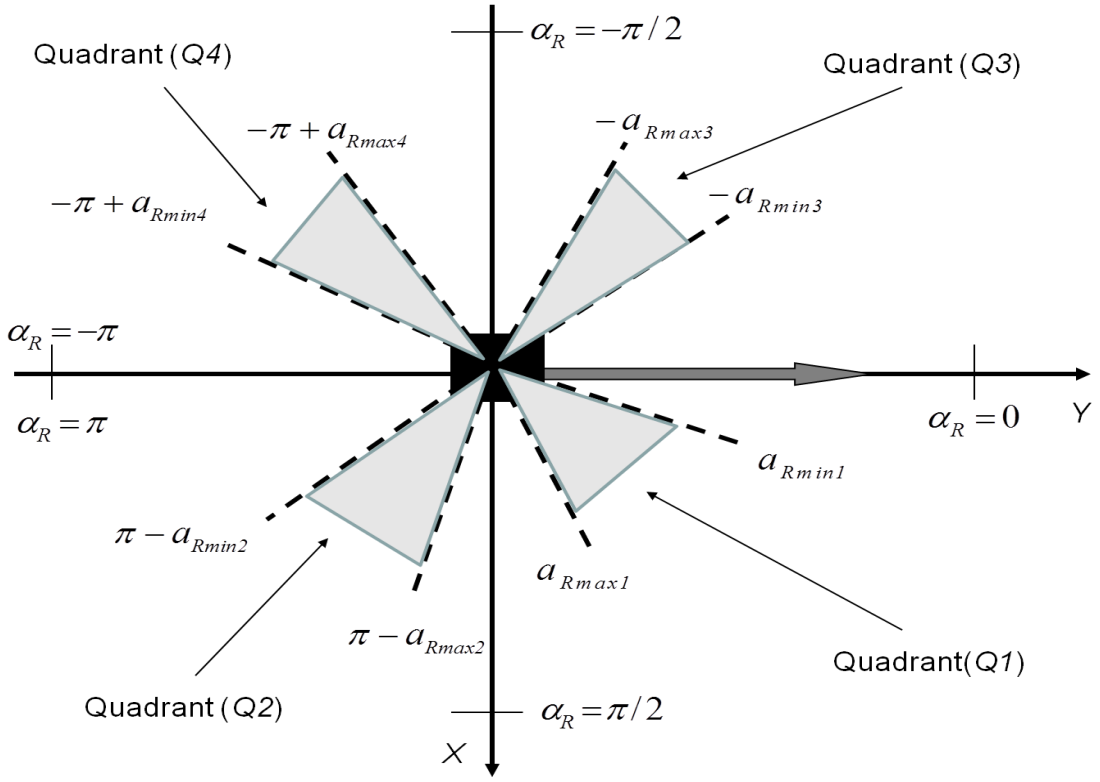

Fig. 6. Azimuth quadrants at the Rx side.

We assume restricted uniform 3-D scattering at both the Tx and Rx sides, where multipath power departs (arrives) from (at) sector $S_{T(R)}$: $A_{T(R)min} \le \alpha_{T(R)} \le A_{T(R)max}$ and $B_{T(R)min} \le \beta_{T(R)} \le B_{T(R)max}$ (see Fig. 5). $A_{T(R)min}$ and $A_{T(R)max}$ are the minimum and maximum azimuth AOD (AOA) with $-\pi \le A_{T(R)min} \le A_{T(R)max} \le \pi$. $B_{T(R)min}$ and $B_{T(R)max}$, are the minimum and maximum elevation AOD (AOA) with $-\pi/2 \le B_{T(R)min} \le B_{T(R)max} \le \pi/2$. Thus, we have for the AOD (AOA) PDF [63]

$$p_{\alpha_{T(R)}}(\alpha_{T(R)}) p_{\beta_{T(R)}}(\beta_{T(R)}) = \frac{\cos\beta_{T(R)max}}{(sinB_{T(R)max} - sinB_{T(R)min})(A_{T(R)max} - A_{T(R)min})}. \quad (27)$$

The usefulness in defining such a uniform 3-D scattering sector will become evident below in the derivation of the PSD, LCR and AFD. From equation (27), the ACF in equation (25) can be written as [64]

$$R_{T(R)}(\Delta t) = U_{T(R)} \int_{B_{T(R)min}}^{B_{T(R)max}} \int_{A_{T(R)min}}^{A_{T(R)max}} cos\beta_{T(R)} exp(j2\pi v_{T(R)max} \cos\beta_{T(R)} \cos\alpha_{T(R)} \Delta t) d\alpha_{T(R)} d\beta_{T(R)} \quad (28)$$

where

$$U_{T(R)} = 1/[(sinB_{T(R)max} - sinB_{T(R)min})(A_{T(R)max} - A_{T(R)min})]. \quad (29)$$

Then, assuming α_1 and α_2 to be uniformly distributed in $[-\pi, \pi]$, which can be the case when many mobile scatterers exist in the propagation environment, $R_S(\Delta t)$ in equation (26) will be [65]

$$R_S(\Delta t) = \int_0^\infty p_{u_S}(u_S) J_0^2(2\pi u_S \Delta t / \lambda) du_S \quad (30)$$

where $J_0(.)$ is the Bessel function of first kind and zero order [49, Appendix (A)]. To obtain equation (30), we do not consider the directions of movement of mobile

scatterers, which cannot be totally random in V-V channels as assumed in [47], but we directly model the AOA and AOD of multipath power with respect to scatterers' motion (see Fig. 4). In equation (30), a suitable model for $p_{u_S}(u_S)$, i.e., the diffuse multipath power distributed over u_S, under moderate to heavy automobile traffic conditions in urban environments, was found to be the Weibull PDF with shape parameter $a \leq 1$ [65]. Thus, $p_{u_S}(u_S)$ can be defined as [65]

$$p_{u_S}(u_S) = w u_S^{a-1} \exp(-w u_S{}^a / a) \tag{31}$$

where w is Weibull the scale parameter. Alternative suitable PDFs, were shown to be the Nakagami-*m* (with $m < 1/2$), the gamma and the lognormal. In, [65] the ACF due to scatterers' mobility was determined based on the relevant scattered power. This is different from considering scatterers' velocity distributions (see, e.g., [66] and [67]) and directly applying them to model $p_{u_S}(u_S)$ as in [47]. As demonstrated in [49, Ch. (7)], most multipath power is contributed by the static and slowly moving objects. Thus, the lower velocities will appear with a greater power contribution than the higher ones. Such physical behaviour is guaranteed by the PDF of equation (31), as well as by the other alternative PDFs considered in [65]. Thus, it is essential to model the multipath power distribution over the velocities, rather than the velocity distribution itself.

By taking the Fourier transform of equation (22) with respect to Δt, we find the PSD, $P_{SN}(v)$, of the narrowband V-V channel as follows

$$P_{SN}(v) = S_D(v) + \rho^2 \delta(v - v_{LOS}) \tag{32}$$

where $S_D(v)$ is the Doppler spectrum of the diffuse part defined as

$$S_D(v) = 2\sigma^2 S_T(v) * S_S(v) * S_R(v) \tag{33}$$

where $*$ is the convolution operator and $S_{T(R)}(v)$ and $S_S(v)$ represent the PSDs due to a) scattering around the Tx (Rx) and b) scatterers' mobility, respectively. They

arise after taking the Fourier transforms of the ACFs in equations (28) and (30), respectively.

The PSD due to scattering around the Tx (Rx) will be [64]

$$S_{T(R)}(v)=\frac{U_{T(R)}}{2v_{T(R)max}}\begin{cases}arcsin\dfrac{v^2(sin^2A_{T(R)max}+1)-v_{T(R)max}^2cos^2A_{T(R)max}}{(v_{T(R)max}^2-v^2)cos^2A_{T(R)max}}-\\ arcsin\dfrac{v^2(sin^2A_{T(R)min}+1)-v_{T(R)max}^2cos^2A_{T(R)min}}{(v_{T(R)max}^2-v^2)cos^2A_{T(R)min}},\\ v_{T(R)max}cosA_{T(R)min}\cos B_{T(R)max}\le v\le v_{T(R)max}cosA_{T(R)max}\cos B_{T(R)min}\\ arcsin\dfrac{v_{T(R)max}^2cos(2B_{T(R)min})-v^2}{v_{T(R)max}^2-v^2}-\\ arcsin\dfrac{v^2(sin^2A_{T(R)min}+1)-v_{T(R)max}^2cos^2A_{T(R)min}}{(v_{T(R)max}^2-v^2)cos^2A_{T(R)min}},\\ max(v_{T(R)max}cosA_{T(R)min}cosB_{T(R)max},v_{T(R)max}cosA_{T(R)max}cosB_{T(R)min})\\ \le v\le v_{T(R)max}cosA_{T(R)min}cosB_{T(R)min}\\ arcsin\dfrac{v^2(sin^2A_{T(R)max}+1)-v_{T(R)max}^2cos^2A_{T(R)max}}{(v_{T(R)max}^2-v^2)cos^2A_{T(R)max}}-\\ arcsin\dfrac{v_{T(R)max}^2cos(2B_{T(R)max})-v^2}{v_{T(R)max}^2-v^2},\\ v_{T(R)max}cosA_{T(R)max}cosB_{T(R)max}\le v\le\\ min(v_{T(R)max}cosA_{T(R)min}cosB_{T(R)max},v_{T(R)max}cosA_{T(R)max}cosB_{T(R)min})\\ arcsin\dfrac{v_{T(R)max}^2cos(2B_{T(R)min})-v^2}{v_{T(R)max}^2-v^2}-\\ arcsin\dfrac{v_{T(R)max}^2cos(2B_{T(R)max})-v^2}{v_{T(R)max}^2-v^2},\\ v_{T(R)max}cosA_{T(R)max}cosB_{T(R)min}\le v\le v_{T(R)max}cosA_{T(R)min}cosB_{T(R)max}\\ \\ 0,otherwise\end{cases} \tag{34}$$

Equation (34) holds when $0\le A_{T(R)min}\le\alpha_{T(R)}\le A_{T(R)max}\le\pi/2$ (azimuth quadrant *Q1*, see Fig. 6) and $0\le B_{T(R)min}\le\beta_{T(R)}\le B_{T(R)max}\le\pi/2$ (positive elevation AOD (AOA)). For negative elevation AOD (AOA), i.e., $-\pi/2\le B_{T(\mathrm{R})min}\le\beta_{T(\mathrm{R})}\le B_{T(\mathrm{R})max}\le 0$, we

just need to define $-\pi/2 \le \underbrace{-b_{T(\mathrm{R})max}}_{B_{T(\mathrm{R})min}} \le \beta_{T(\mathrm{R})} \le \underbrace{-b_{T(\mathrm{R})min}}_{B_{T(\mathrm{R})max}} \le 0$. Then, due to the even symmetry of the cosine function, the PSD will arise from equation (34) by substituting $B_{T(\mathrm{R})min} \to b_{T(\mathrm{R})min}$ and $B_{T(\mathrm{R})max} \to b_{T(\mathrm{R})max}$.

We also have the following cases regarding the azimuth AOD (AOA) [64]:

a) If $\pi/2 \le A_{T(R)min} \le \alpha_{T(R)} \le A_{T(R)max} \le \pi$ (azimuth quadrant *Q2*, see Fig. 6), we need to define $\pi/2 \le \underbrace{\pi - a_{T(\mathrm{R})max2}}_{A_{T(R)min}} \le \alpha_{T(R)} \le \underbrace{\pi - a_{T(\mathrm{R})min2}}_{A_{T(R)max}} \le \pi$. Then, the PSD will arise from equation (34) by making the following substitutions, $v \to -v$, $A_{T(R)min} \to a_{T(\mathrm{R})min2}$ and $A_{T(R)max} \to a_{T(\mathrm{R})max2}$.

b) If $-\pi/2 \le A_{T(R)min} \le \alpha_{T(R)} \le A_{T(R)max} \le 0$ (azimuth quadrant *Q3*, see Fig. 6), we need to define $-\pi/2 \le \underbrace{-a_{T(\mathrm{R})max3}}_{A_{T(R)min}} \le \alpha_{T(R)} \le \underbrace{-a_{T(\mathrm{R})min3}}_{A_{T(R)max}} \le 0$. Then, the PSD will arise from equation (34) by making the following substitutions, $A_{T(R)min} \to a_{T(\mathrm{R})min3}$ and $A_{T(R)max} \to a_{T(\mathrm{R})max3}$.

c) If $-\pi \le A_{T(R)min} \le \alpha_{T(R)} \le A_{T(R)max} \le -\pi/2$ (azimuth quadrant *Q4*, see Fig. 6), we need to define $-\pi \le \underbrace{-\pi + a_{T(\mathrm{R})min4}}_{A_{T(R)min}} \le \alpha_{T(R)} \le \underbrace{-\pi + a_{T(\mathrm{R})max4}}_{A_{T(R)max}} \le -\pi/2$. Then, the PSD will arise from equation (34) by making the following substitutions $v \to -v$, $A_{T(R)min} \to a_{T(\mathrm{R})min4}$ and $A_{T(R)max} \to a_{T(\mathrm{R})max4}$.

It is now evident why defining uniform sectors for the AOD and AOA is very useful. First, we have analytical solutions for the PSDs at the Tx and Rx sides and moreover, there is a theoretical flexibility to incorporate any 3-D scattering scenario by considering AOD and AOA PDFs composed by weighted uniform contributions in different sectors (having the form of equation (27), see [63] and [64]). Then, the PSDs contributed by each sector can be analytically determined as in equation (34) and taking into account the relevant azimuth quadrant as described above.

The PSD due to scatterers' mobility will be [65]

$$S_S(v) = \int_0^{\infty} p_{u_S}(u_S)\xi(v,u_S)du_S \tag{35}$$

where

$$\xi(v,u_S)=\begin{cases}\dfrac{\lambda}{\pi^2 u_S}K\left[\sqrt{1-\left(\dfrac{v\lambda}{2u_S}\right)^2}\right], |v|\le\dfrac{2u_S}{\lambda}\\ 0, otherwise\end{cases} \tag{36}$$

with $K(.)$ being the complete elliptic integral of the first kind [68, Ch. (8)].

Fig. 7 presents PSDs from equation (33) for several V-V channel scenarios. The parameter set is considered in order to have PSDs with: a) positive Doppler frequencies only (Fig. 7a), b) negative Doppler frequencies only (Fig. 7b), and c) both positive and negative Doppler frequencies (Fig. 7c). We also consider the impact of scatterers, mobility by varying its intensity through the parameter w in equation (31). More specifically, from equation (A6) in Appendix, we see that if w decreases, W_2 (the second moment of the Weibull random variable used to describe $p_{u_S}(u_S)$) increases, making the scatterers' mobility more intense because the mean value and variance of u_S increase (see [65], [69, Table (5-2)] and also Fig. 8). In Fig. 7a (Q1Q1 scenario), departure and arrival take place within quadrant *Q1*, with $A_{Tmin}=\pi/9$, $A_{Tmax}=\pi/3$ and $A_{Rmin}=\pi/12$, $A_{Rmax}=\pi/4$. In Fig. 7b (Q2Q2 scenario), departure and arrival take place within quadrant *Q2*, with $A_{Tmin}=\pi-\pi/9=8\pi/9$, $A_{Tmax}=\pi-\pi/3=2\pi/3$ and $A_{Rmin}=\pi-\pi/12=11\pi/12$, $A_{Rmax}=\pi-\pi/4=3\pi/4$. In Fig. 7c (Q1Q2 scenario), departure and arrival take place within quadrant *Q1*, with $A_{Tmin}=\pi/9$, $A_{Tmax}=\pi/3$ and within quadrant *Q2*, with $A_{Rmin}=\pi-\pi/12=11\pi/12$, $A_{Rmax}=\pi-\pi/4=3\pi/4$, respectively. See Fig. 6 for a schematic representation of quadrants. The remaining parameters are defined as $B_{Tmin}=B_{Rmin}=0$ in both Tx and Rx quadrants, $B_{Tmax}=\pi/6$ in both Tx quadrants, $B_{Rmax}=\pi/9$ in both Rx quadrants, $a=0.75$, $2\sigma^2=1$ and $f_{Tmax}=f_{Rmax}=100Hz$. As is shown in Fig. 7, the PSD is asymmetric in general. Higher Doppler frequencies than those predicted when considering only the Tx and Rx mobility appear due to the impact of scatterers' mobility. This effect becomes more intense as the scatterers' mobility increases (i.e., when more power is scattered by mobile scatterers). Fig. 8 presents the Weibull PDFs

for the power distributed over the scatterers' velocities (equation (31)) for the parameter set of Fig. 7 ($a = 0.75$ and $w = 1, 2$).

Two more well-known metrics when dealing with second order statistical characterization are the LCR and AFD. Their importance is well-known for a variety of applications, such as determining the frame length for coded systems [70] and estimating the throughput of communication protocols [71]. We first consider the LCR, $N(z)$, being the average number of crossings per second that $G_N(t)$ crosses a specified signal level z, with positive slope. For a Rician channel, the LCR is [72, Ch. (6)]

$$N(z) = \frac{z\sqrt{2d_1}}{\pi^{3/2}\psi_0}\exp\left(-\frac{z^2+\rho^2}{2\psi_0}\right)\times \int_0^{\pi/2}\left\{\exp[-(d_2\rho\sin\theta)^2] + \sqrt{\pi}d_2\rho\sin\theta\cdot erf(d_2\rho\sin\theta)\right\}\cosh\left(\frac{z\rho\cos\theta}{\psi_0}\right)d\theta \quad (37)$$

where $erf(.)$ is the error function [72, Ch. (3)]. Under the absence of LOS ($\rho = 0$), with only diffuse multipath propagation, the LCR becomes

$$N(z) = \sqrt{d_1/(2\pi)}\exp[-z^2/(2\psi_0)]\cdot z/\psi_0 \quad (38)$$

The following parameters should be further determined in equations (37) and (38), namely, $\psi_0 = R_D(0)/2$, $\phi_{01} = \mathrm{Im}[R_D'(0)]/2$ and $\psi_{02} = R_D''(0)/2$, where the primes denote derivatives with respect to Δt and Im[.] refers to the imaginary part of the bracketed term. These parameters will be (see Appendix for equations (40) and (41))

$$\psi_0 = \sigma^2 \quad (39)$$

$$\phi_{01} = \pi\sigma^2(v_{Tmax}U_TQ_T + v_{Rmax}U_RQ_R) \quad (40)$$

$$\psi_{02} = \pi^2\sigma^2[(v_{Tmax}^2U_TY_T/6) + (v_{Rmax}^2U_RY_R/6) - 4W_2/\lambda^2 - 2v_{Tmax}U_TQ_Tv_{Rmax}U_RQ_R]. \quad (41)$$

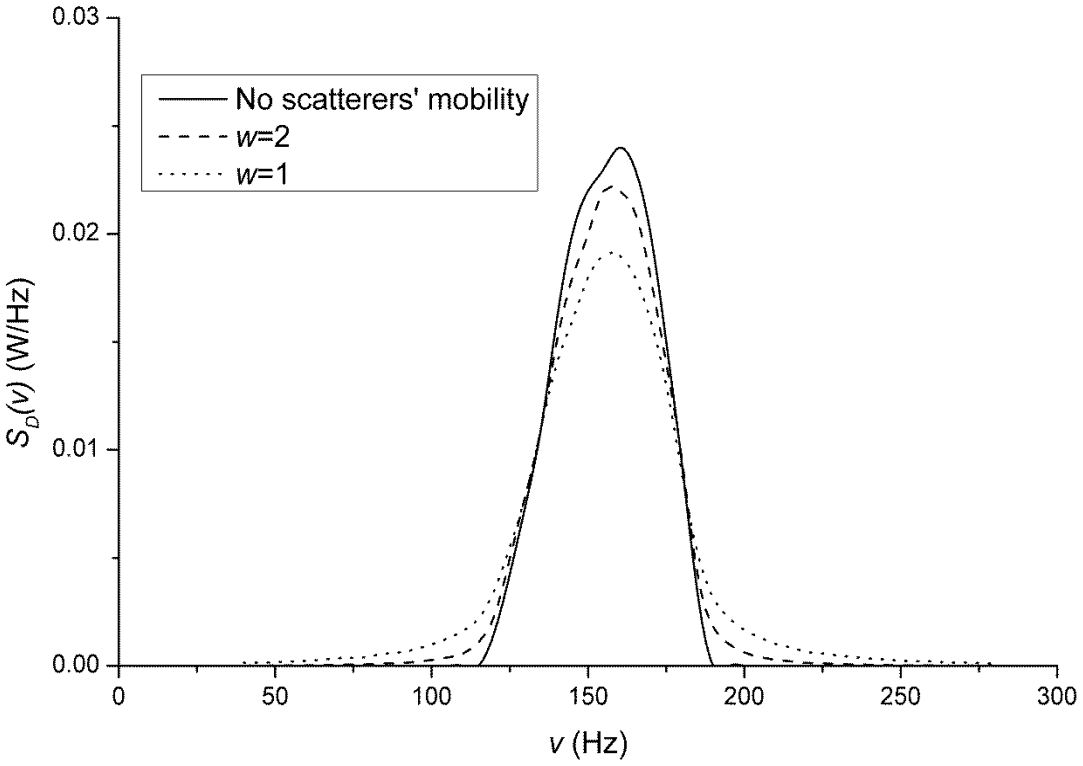
No scatterers' mobility
w=2
w=1
0.03
0.02
0.01
0.00
$S_D(v)$ (W/Hz)
0
50
100
150
200
250
300
v (Hz)

a

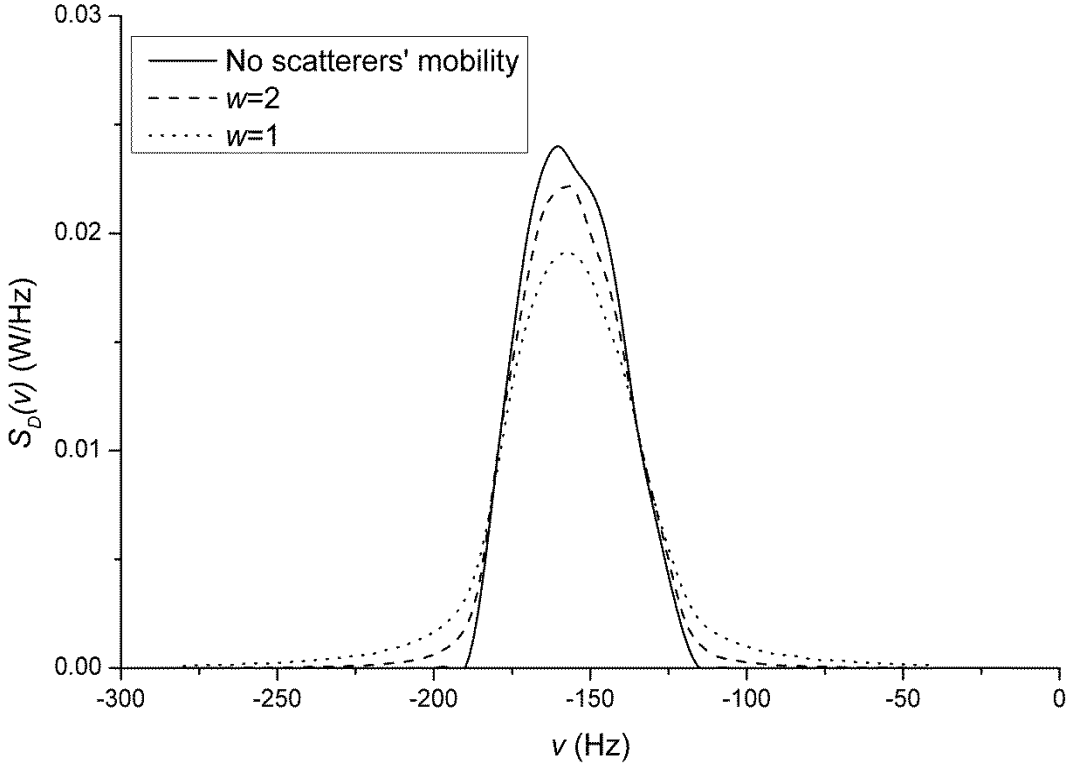
No scatterers' mobility
w=2
w=1
0.03
0.02
0.01
0.00
$S_D(v)$ (W/Hz)
-300
-250
-200
-150
-100
-50
0
v (Hz)

b

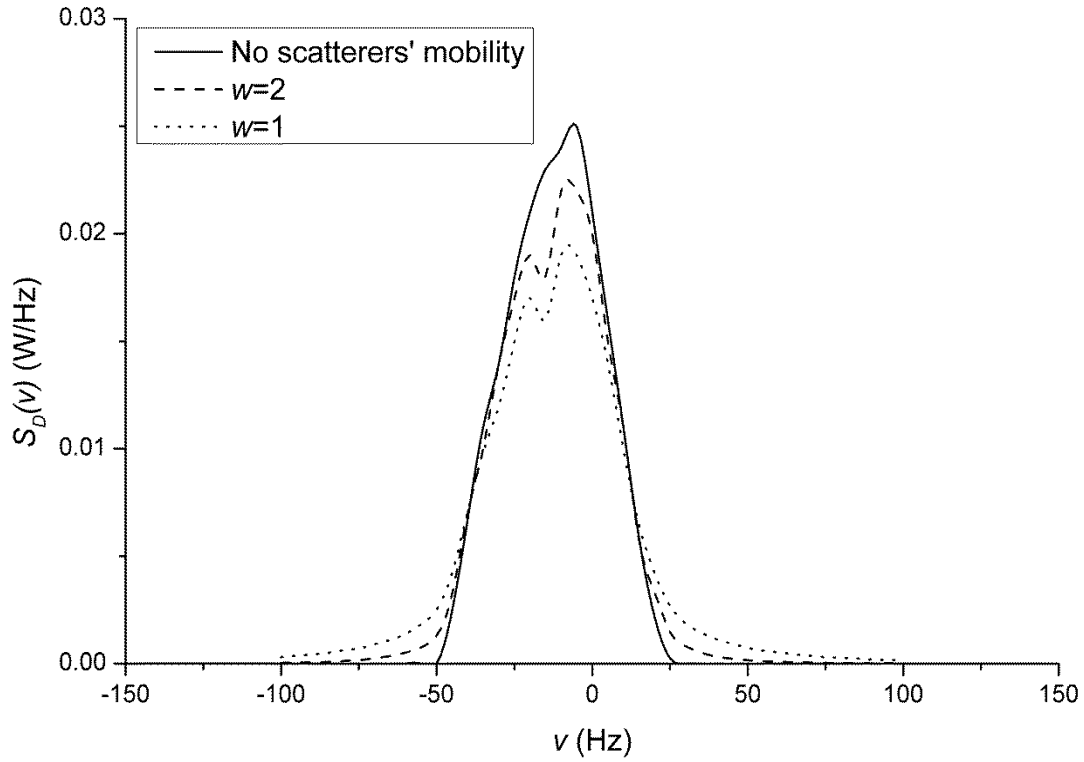

c

Fig. 7. PSD for several V-V channel scenarios: a) Q1Q1, b) Q2Q2, c) Q1Q2.

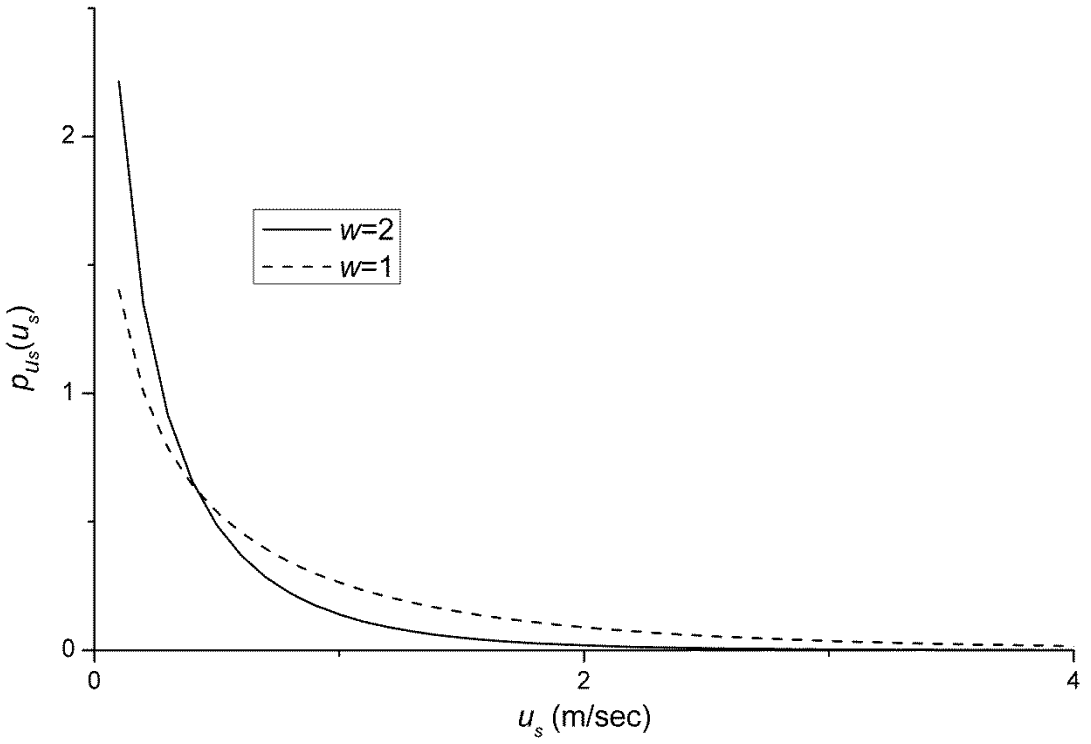

Fig. 8. Weibull PDF for diffuse multipath power distributer over the scatterers' velocities.

The quantities Q_T, Q_R, Y_T, Y_R, W_2 are determined in the Appendix and U_T, U_R are given by equation (29). Moreover, d_1 and d_2 in equations (37) and (38) are defined as [72, Ch. (6)]

$$d_1 = -\psi_{02} - (\phi_{01}^2 / \psi_0) \tag{42}$$

$$d_2 = [2\pi f_{LOS} - (\phi_{01} / \psi_0)] / \sqrt{2d_1}\,. \tag{43}$$

In equation (41), we identify inside the bracket four terms contributing to the temporal variability arisen from different effects that are taking place in the V-V channel. More specifically the terms $v_{Tmax}^2 U_T Y_T / 6$, $v_{Rmax}^2 U_R Y_R / 6$ and $-4W_2 / \lambda^2$ are contributed by the effects of scattering around the Tx (and due to Tx mobility), scattering around the Rx (and due to Rx mobility) and scatterers' mobility, respectively. The cross-term $-2v_{Tmax} U_T Q_T v_{Rmax} U_R Q_R$ arises from the generally asymmetric scattering (and not just anisotropic) at the azimuth plane with respect to the Tx and Rx motion. From equation (A12) or (A16), we can see that this term will be zero (i.e., $Q_T = 0$, or $Q_R = 0$), if either symmetric scattering at the azimuth plane with respect to the Tx motion (with respect to $\alpha_T = 0$), or with respect to the Rx motion (with respect to $\alpha_R = 0$) takes place. Of course, this holds for isotropic scattering too, which is a special case of symmetric scattering. Scattering at the elevation planes has no impact on whether or not $-2v_{Tmax} U_T Q_T v_{Rmax} U_R Q_R$ is zero. If, moreover, symmetric scattering takes place at both azimuth planes around the Tx and Rx, then ϕ_{01} in equation (40) will be zero too. Cross terms arisen from the impact of scatterers' mobility are missing as $R_S'(0) = 0$ (see equation (A3) in Appendix). This occurs because $R_S(\Delta t)$ is a real and even function (see equation (30)) arisen by isotropic scattering around mobile scatterers, i.e., α_1 and α_2 to be uniformly distributed in $[-\pi, \pi]$ (see Fig. 4). The latter leads to a real and even PSD (see equations (35) and (36)), which is a natural result, as we do not anticipate the propagation environment itself to be biased towards positive or negative Doppler frequencies. A similar rationale was also deployed in [49, Ch. (7)], which has been

validated by numerous measurement campaigns of fixed wireless channels (wireless channels with static Tx and Rx and scatterers' mobility as the only source of temporal variability), see related references discussed in [65].

We also consider the AFD, $T(z)$, defined as the mean value of the time intervals that $G_N(t)$ remains below a specified signal level z. The following definition holds for the AFD [72, Ch. (2)]

$$T(z) = \frac{F_{G_N}(z)}{N(z)} \tag{44}$$

where $F_{G_N}(z)$ is the cumulative distribution function (CDF) of $G_N(t)$ defined as

$$F_{G_N}(z) = \int_0^z p_{G_N}(x)dx = 1 - Q_1\left(\sqrt{2K_r}, \sqrt{2(K_r+1)}z/\sqrt{\Omega}\right) \tag{45}$$

where $Q_m(.,.)$ is the generalized Marcum-Q function [72, Ch. (6)], $\Omega = \rho^2 + 2\sigma^2$ the mean power of $G_N(t)$ and $K_r = \rho^2/(2\sigma^2)$ the Rician K-factor.

The LCR and AFD characterize the temporal variability of V-V channels (and generally of all wireless channels). Temporal variability is also characterized by the average Doppler shift, v_a, and the Doppler spread, σ_V, determined as (see Appendix)

$$v_a = (v_{Tmax}U_TQ_T + v_{Rmax}U_RQ_R)/2 \tag{46}$$

$$\sigma_V = \frac{1}{2}\sqrt{-\frac{v_{Tmax}^2U_TY_T}{6} - \frac{v_{Rmax}^2U_RY_R}{6} + \frac{4W_2}{\lambda^2} - (v_{Tmax}U_TQ_T)^2 - (v_{Rmax}U_RQ_R)^2}\,. \tag{47}$$

As a final remark, we point out the usefulness of defining 3-D uniform sectors for the AOD and AOA. First, we obtained closed form solutions for the essential parameters for determining the LCR and AFD (i.e., ϕ_{01} and ψ_{02}). We can theoretically incorporate any 3-D scattering scenario by considering weighted uniform contributions in different sectors and then, solving for ϕ_{01} and ψ_{02}, will always lead

us to similar integrals as in the right sides of equations (A16) and (A18), which are analytically determined.

In order to determine the impact of the different effects taking place on the time variability of the V-V channel, we plot in Fig. 9 the normalized LCR $N(z)/(v_{Tmax}+v_{Rmax})$ with $\rho=0$ (i.e., that in equation (38)) by parameterizing: a) the scatterers' mobility through w (Fig. 9a) , b) the azimuth AOD through A_{Tmax} (Fig. 9b), and c) the elevation AOD through B_{Tmax} (Fig. 9c). We have considered the following parameter set: $a=0.75$, $2\sigma^2=1$ and $f_{Tmax}=f_{Rmax}=100Hz$, $A_{Tmin}=A_{Rmin}=-\pi$, $B_{Tmin}=B_{Rmin}=-\pi/2$, $A_{Rmax}=-3\pi/4$ and $B_{Rmax}=-\pi/4$. Moreover, in Fig. 9a, we have $A_{Tmax}=-3\pi/4$, $B_{Tmax}=-\pi/4$, in Fig. 9b, $B_{Tmax}=-\pi/4$, $w=2$ and in Fig. 9c, $A_{Tmax}=-3\pi/4$, $w=2$. It is clear from Fig. 9a that when the scatterers' mobility becomes more intense (w decreases), the LCR increases, thus, temporal fluctuations become more frequent. From Fig. 9b, we see that when the multipath spread in the azimuth plane increases (A_{Tmax} increases), the LCR increases and thus, fluctuations occur more frequently. However, an important increase is observed when the polarity of the azimuth AODs is maintained (negative AODs). An interesting behaviour is revealed in Fig. 9c when the multipath spread in the elevation plane increases. More specifically, if the multipath spread in the elevation plane increases maintaining its polarity (i.e., having only negative or positive elevation AODs), the LCR increases and reaches a maximum when the elevation spread is maximum at $B_{Tmax}=0$. Any further increase, which results elevation AODs with positive sign, will reduce the LCR, which will reach its maximum when the multipath spread becomes maximum at $B_{Tmax}=\pi/2$. The meaning is that the existence of some negative elevation AODs topped up on the positive ones (and vice versa), can reduce the LCR and thus the temporal variations. Similar results will be obtained if we consider the azimuth and elevation AOA.

V. MODEL VALIDATION

Our modeling approach lays its strength in offering a theoretical flexibility to account for any 3-D scattering scenario at the Tx and Rx sides by considering weighted uniform contributions in different angular sectors. Then, the PSDs

contributed by each sector can be analytically determined as in equation (34). The incorporation of the scatterers' mobility impact, further generalizes our modeling approach and the LCR and AFD can be determined by well-know formulas such as equations (37) and (44).

However, in this section, we further demonstrate the flexibility and usefulness of our approach by adapting the theoretical LCR to empirical presented in [16]. The measurement environments were an urban street area and a US interstate highway. Here, we consider the LCR from the interstate highway environment. Our task is to find the optimal values of the model parameter vector $V = [A_{Tmin}\ A_{Tmax}\ B_{Tmin}\ B_{Tmax}\ A_{Rmin}\ A_{Rmax}\ B_{Rmin}\ B_{Rmax}\ w\ a]^T$, such that the absolute value of the difference between the analytical and measured LCRs is minimum. In order to do so, we insert the model parameters to a multi-parametric function, seeking its minimum. That function is

$$\Upsilon(V) = \left(\sum_{i=1}^{M} \left[\left(\frac{N(z_i) - N_m(z_i)}{N_m(z_i)} \right)^2 \right] \right)^{1/2} \tag{48}$$

where $N_m(z_i)$ is the measured LCR at signal level z_i and M is the number of measured values. The remaining parameter are determined from [16] as $2\sigma^2 = 1$, $\rho = 1.136$, $v_{LOS} = 0$ and $f_{Tmax} = f_{Rmax} = 181.72Hz$, By minimizing $\Upsilon(V)$, we find the parameter set given in table I. The resulting analytical and measured normalized LCRs $N(z)/v_{Tmax}$ and $N_m(z)/v_{Tmax}$, respectively, are shown in Fig. 10, where a very good agreement between them is revealed.

TABLE I

THEORETICAL MODEL PARAMETERS

A_{Tmin}	A_{Tmax}	B_{Tmin}	B_{Tmax}	A_{Rmin}	A_{Rmax}	B_{Rmin}	B_{Rmax}	w	a
$\frac{-\pi}{7.826}$	$\frac{\pi}{4.186}$	$\frac{-\pi}{71.4}$	$\frac{-\pi}{35.7}$	$\frac{\pi}{3.915}$	$\frac{\pi}{2.093}$	$\frac{-\pi}{31.733}$	$\frac{\pi}{35.7}$	0.63	1

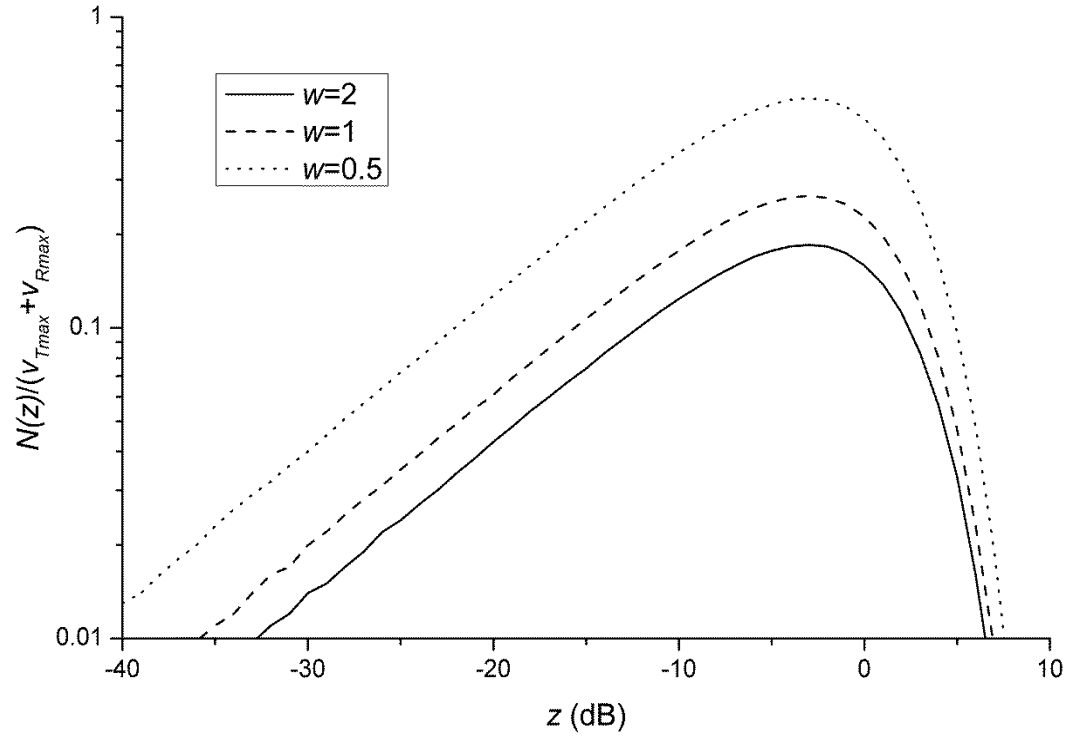
w=2
w=1
w=0.5
N(z)/(v_Tmax+v_Rmax)
1
0.1
0.01
-40
-30
-20
-10
0
10
z (dB)

a

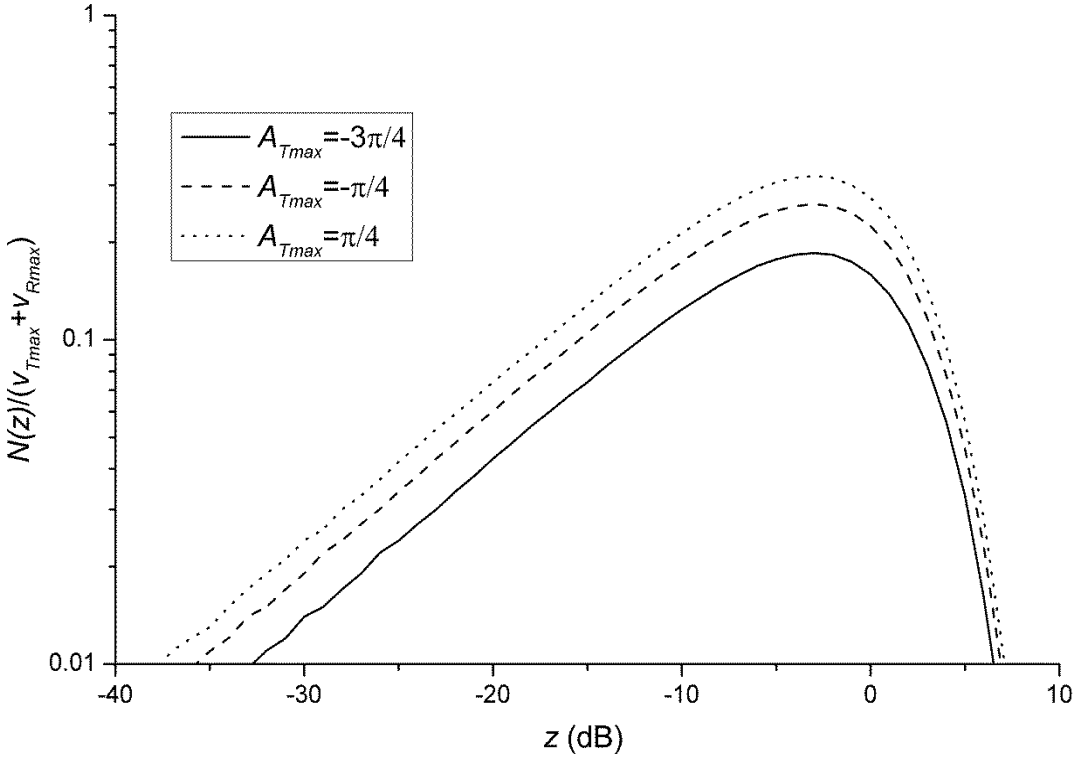
A_Tmax=-3π/4
A_Tmax=-π/4
A_Tmax=π/4
N(z)/(v_Tmax+v_Rmax)
1
0.1
0.01
-40
-30
-20
-10
0
10
z (dB)

b

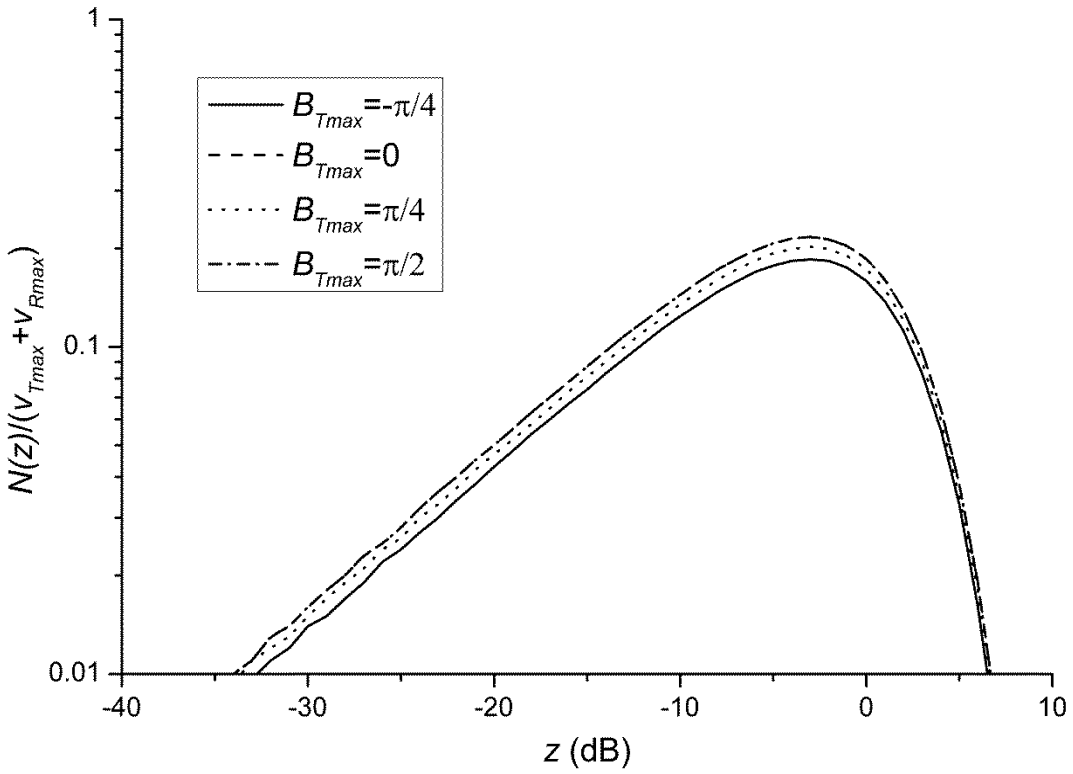

c

Fig. 9. LCR for several V-V channel scenarios with respect to: a) scatterers' mobility, b) azimuth AOD, c) elevation AOD.

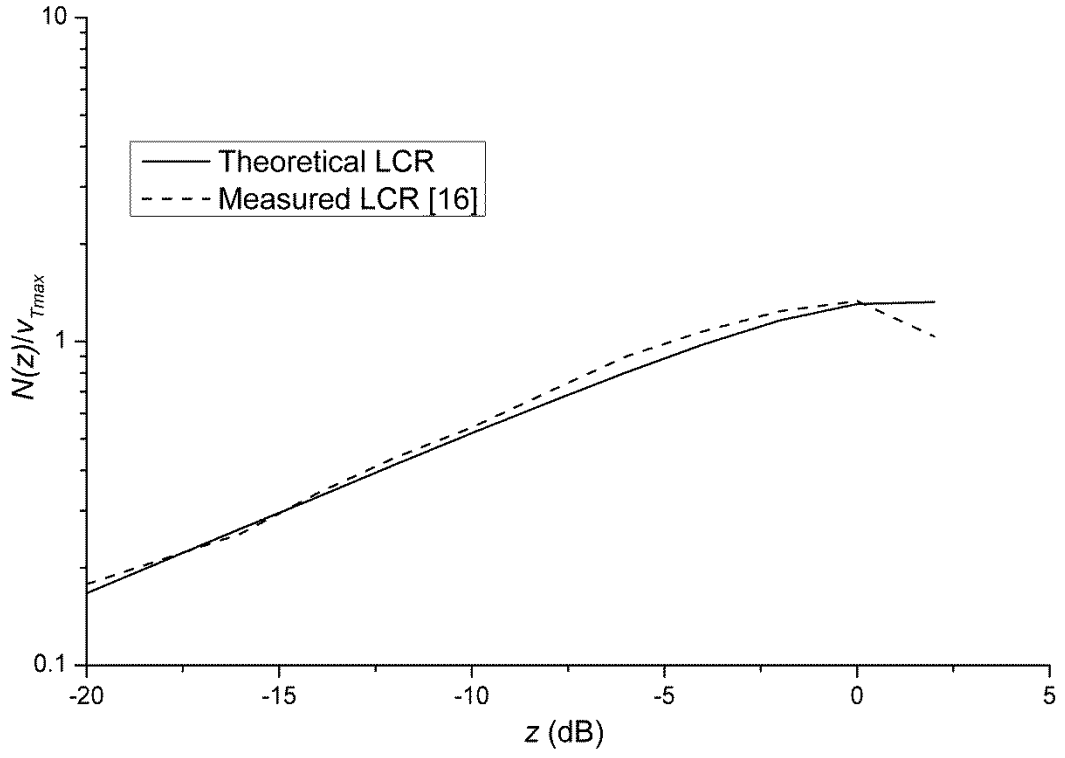

Fig. 10. Theoretical and measured LCR on an interstate highway.

VI. CONCLUSION

A V-V stochastic channel model was considered based on the DU property of realistic non-WSSUS wireless channels. Focus was given on characterizing the temporal variability of the channel through the determination of the second order statistics, namely, the a) ACF, b) PSD, c) LCR and d) AFD. 3-D scattering was considered at both the Tx and Rx sides together with random scatterers' mobility (e.g., other vehicles). The model exhibits a theoretical flexibility to account for any 3-D scattering scenario. Its applicability is restricted within the stationarity time and stationarity frequency intervals, i.e., within the RTI and RBW, respectively. Thus it accounts for small scale variations of V-V channels. It is possible though to proceed to develop composite stochastic models that include large scale variations (variations outside the RTI and RBW) in addition to the small scale ones. We demonstrated that scatterers' mobility can induce higher Doppler frequencies than those predicted when considering the Tx and Rx mobility only. With more intense scatterers' mobility the temporal variability increases. In general, the same holds when multipath propagation becomes less directional. Curve-fitting of the theoretical LCR to an empirical obtained at a US interstate highway with anticipated intense scatterers' mobility, further demonstrated the usefulness and flexibility of our modeling approach.

APPENDIX-DERIVATION OF EQUATIONS (40), (41), (46), (47)

The first order derivative of $R_D(\Delta t)$ with respect to Δt will be

$$R_D' = 2\sigma^2 (R_S' R_T R_R + R_T' R_S R_R + R_R' R_S R_T)\,. \tag{A1}$$

The second order derivative will be

$$\begin{aligned} R_D'' = 2\sigma^2 (&R_S'' R_T R_R + R_S' R_T' R_R + R_S' R_T R_R' + \\ &R_T'' R_S R_R + R_T' R_S' R_R + R_T' R_S R_R' + R_R'' R_S R_T + R_R' R_S' R_T + R_R' R_S R_T') \end{aligned} \tag{A2}$$

where, for simplicity, we omitted the argument Δt from equations (A1) and (A2).

Next, with the aid of [68, eq. (8.473-4)], we have from equation (30)

$$R'_S(\Delta t) = -(4\pi/\lambda)\int_0^\infty J_0(2\pi u_S \Delta t/\lambda) J_1(2\pi u_S \Delta t/\lambda) u_S p_{u_S}(u_S) du_S = 0\big|_{\Delta t=0} \quad \text{(A3)}$$

where $J_1(.)$ is the Bessel function of first kind and first order [49, Appendix (A)]. Next, with the aid of [68, eqs. (8.472-1) and (8.472-2)], we can show that $J'_1(\Delta t) = [J_0(\Delta t) - J_2(\Delta t)]/2$, where $J_2(.)$ is the Bessel function of first kind and second order [49, Appendix (A)]. Thus, we have from equation (A3)

$$R''_S(\Delta t) = -(8\pi^2/\lambda^2) \times \int_0^\infty u_S^2 p_{u_S}(u_S) \times$$
$$\left[-J_1^2(2\pi u_S \Delta t/\lambda) + J_0(2\pi u_S \Delta t/\lambda) \frac{J_0(2\pi u_S \Delta t/\lambda) - J_2(2\pi u_S \Delta t/\lambda)}{2} \right] du_S . \quad \text{(A4)}$$

We have from equation (A4)

$$R''_S(0) = -(4\pi^2/\lambda^2)\int_0^\infty u_S^2 p_{u_S}(u_S) du_S = -(4\pi^2/\lambda^2) W_2 \quad \text{(A5)}$$

where $W_2 = W_1^2 + \sigma_W^2$ is the second moment of the Weibull random variable, which models $p_{u_S}(u_S)$ in equation (31), with W_1 and σ_W^2 its mean and variance, respectively. Using their respective formulas from [69, Table 5-2], we have

$$W_2 = (a/w)^{2/a} \Gamma[1 + (2/a)] \quad \text{(A6)}$$

where $\Gamma(.)$ is the gamma function [49, Appendix (A)].

Next, we write the ACFs in equation (28) as

$$R_{T(R)}(\Delta t) = C_{T(R)}(\Delta t) + jD_{T(R)}(\Delta t) \quad \text{(A7)}$$

where

$$C_{T(R)}(\Delta t) = U_{T(R)} \int_{B_{T(R)min}}^{B_{T(R)max}} \int_{A_{T(R)min}}^{A_{T(R)max}} cos\beta_{T(R)} cos(j2\pi v_{T(R)max} \cos\beta_{T(R)} \cos\alpha_{T(R)} \Delta t) d\alpha_{T(R)} d\beta_{T(R)} \tag{A8}$$

$$D_{T(R)}(\Delta t) = U_{T(R)} \int_{B_{T(R)min}}^{B_{T(R)max}} \int_{A_{T(R)min}}^{A_{T(R)max}} cos\beta_{T(R)} sin(j2\pi v_{T(R)max} \cos\beta_{T(R)} \cos\alpha_{T(R)} \Delta t) d\alpha_{T(R)} d\beta_{T(R)} \tag{A9}$$

We have from equation (A1) using equation (A3)

$$R'_D(0) = 2\sigma^2[R'_T(0) + R'_R(0)] = 2\sigma^2[C'_T(0) + C'_R(0) + j(D'_T(0) + D'_R(0)]. \tag{A10}$$

As $\phi_{01} = \mathrm{Im}[R'_D(0)]/2$, we have

$$\phi_{01} = \sigma^2[D'_T(0) + D'_R(0)] \tag{A11}$$

After some elementary algebraic manipulations, we can show from equation (A9) that

$$D'_{T(R)}(0) = 2\pi v_{T(R)max} U_{T(R)} \int_{A_{T(R)min}}^{A_{T(R)max}} cos\alpha_{T(R)} d\alpha_{T(R)} \int_{B_{T(R)min}}^{B_{T(R)max}} cos^2\beta_{T(R)} d\beta_{T(R)} \tag{A12}$$

where using [68, eq. (2513-11)], we take

$$D'_{T(R)}(0) = \pi v_{T(R)max} U_{T(R)} Q_{T(R)} \tag{A13}$$

where

$$Q_{T(R)} = (sinA_{T(R)max} - sinA_{T(R)min}) \times$$
$$(B_{T(R)max} - B_{T(R)min} + sinB_{T(R)max} cosB_{T(R)max} - sinB_{T(R)min} cosB_{T(R)min}) \tag{A14}$$

Finally, using equation (A13) in (A11), equation (40) arises.

Next, we have from equation (A2) using equation (A3)

$$R_D''(0) = 2\sigma^2[R_S''(0) + R_T''(0) + R_R''(0) + 2R_T'(0)R_R'(0)]. \quad \text{(A15)}$$

After some elementary algebraic manipulations, we have from equation (28)

$$R_{T(R)}'(0) = j2\pi v_{T(R)max} U_{T(R)} \int_{A_{T(R)min}}^{A_{T(R)max}} cos\alpha_{T(R)} d\alpha_{T(R)} \int_{B_{T(R)min}}^{B_{T(R)max}} cos^2\beta_{T(R)} d\beta_{T(R)} \quad \text{(A16)}$$

where using [68, eq. (2513-11)], we take

$$R_{T(R)}'(0) = j\pi v_{T(R)max} U_{T(R)} Q_{T(R)}. \quad \text{(A17)}$$

We can also show from equation (28)

$$R_{T(R)}''(0) = -4\pi^2 v_{T(R)max}^2 U_{T(R)} \int_{A_{T(R)min}}^{A_{T(R)max}} cos^2\alpha_{T(R)} d\alpha_{T(R)} \int_{B_{T(R)min}}^{B_{T(R)max}} cos^3\beta_{T(R)} d\beta_{T(R)} \quad \text{(A18)}$$

where using [68, eqs. (2513-11) and (2513-12)], we take

$$R_{T(R)}''(0) = \pi^2 v_{T(R)max}^2 U_{T(R)} Y_{T(R)} / 6 \quad \text{(A19)}$$

where

$$Y_{T(R)} = [sin(2A_{T(R)min}) - sin(2A_{T(R)max}) + 2A_{T(R)min} - 2A_{T(R)max}] \times$$
$$[sinB_{T(R)max}(cos(2B_{T(R)max}) + 5) - sinB_{T(R)min}(cos(2B_{T(R)min}) + 5)]. \quad \text{(A20)}$$

Finally, considering $\psi_{02} = R_D''(0)/2$ and using equations (A5), (A17) and (A19) in (A15), equation (41) arises.

The average Doppler shift and Doppler spread are defined as [72, Ch. (3)]

$$v_a = \frac{\int_{-\infty}^{\infty} vS_D(v)dv}{\int_{-\infty}^{\infty} S_D(v)dv} = \frac{R'_D(0)}{2\pi jR_D(0)} \tag{A21}$$

$$\sigma_V = \sqrt{\frac{\int_{-\infty}^{\infty} (v-v_a)^2 S_D(v)dv}{\int_{-\infty}^{\infty} S_D(v)dv}} = \frac{1}{2\pi}\sqrt{\left(\frac{R'_D(0)}{R_D(0)}\right)^2 - \frac{R''_D(0)}{R_D(0)}}\,. \tag{A22}$$

Using equation (A10) in (A21), with the aid of equation (A17), equation (46) arises. Using equation (A15) in (A22), with the aid of equations (A5), (A17) and (A19), equation (47) arises.

REFERENCES

[1] G. Karagiannis, O. Altintas, E. Ekici, G. Heijenk, B. Jarupan, K. Lin, T. Weil, "Vehicular Networking: A Survey and Tutorial on Requirements, Architectures, Challenges, Standards, and Solutions," IEEE Commun. Surveys and Tutorials, vol. 13, no. 4, pp. 584-616, Fourth Quarter, 2011.

[2] IEEE Veh. Technol. Magazine, Special Issue on V2V Communications, vol. 2, no. 4, Dec. 2007.

[3] American Society for Testing and Materials, ASTM E2213, "Standard Specification for Telecommunications and Information Exchange Between Roadside and Vehicle Systems—5GHz Band Dedicated Short Range Communications (DSRC) Medium Access Control (MAC) and Physical Layer (PHY) Specifications," http://www.astm.org, 2008.

[4] IEEE, "IEEE Wireless Access in Vehicular Environments," http://grouper.ieee.org/groups/802/11/Reports/tgp_update.htm, 2014.

[5] R. A. Uzcategui, G. Acosta-Marum, "WAVE: A Tutorial," IEEE Commun. Magazine, vol. 47, no. 5, pp. 126-133, May 2009.

[6] J. D. Parsons, "The Mobile Radio Propagation Channel," 2nd ed., Wiley, 2000.

[7] J. Maurer, T. Fugen and W. Wiesbeck, "Narrow-Band Measurement and Analysis of the Inter-Vehicle Transmission Channel," IEEE Veh. Technol. Conf. (VTC), pp. 1274-1278, May 2002.

[8] J. Maurer, T. Schafer and W. Wiesbeck, "A Realistic Description of the Environment for Inter-Vehicle Wave Propagation Modeling," IEEE Veh. Technol. Conf. (VTC), pp. 1437-1441, Oct. 2001

[9] J. Maurer, T. Fugen, T. Schafer and W. Wiesbeck, "A New Inter-Vehicle Communications (IVC) Channel Model," IEEE Veh. Technol. Conf. (VTC), pp. 9-13, Sep. 2004.

[10] Z. Sun and I. A. Akyildiz, "A Mode-Based Approach for Channel Modeling in Underground Tunnels under the Impact of Vehicular Traffic Flow," IEEE Trans. Wirel. Commun., vol. 10, no. 10, pp. 3222-3231, Oct. 2011.

[11] M. Patzold, B. O. Hogstad and N. Youssef, “Modeling, Analysis and Simulation of MIMO Mobile-to-Mobile Fading Channels,” IEEE Trans. Wirel. Commun., vol. 7, no. 2, pp. 510-520, Febr. 2008.

[12] A. G. Zajic and G. L. Stuber, “Space-Time Correlated Mobile-to-Mobile Channels: Modeling and Simulation,” IEEE Trans. Veh. Technol., vol. 57, no. 2, pp. 715-726, Mar. 2008.

[13] X. Cheng, C. X. Wang, D. I. Laurenson, S. Salous and A. V. Vasilakos, “An Adaptive Geometry-Based Stochastic Model for Non-Isotropic MIMO Mobile-to-Mobile Fading Channels,” IEEE Trans. Wirel. Commun., vol. 8, no. 9, pp. 4824-4835, Sep. 2009.

[14] M. Walter, D. Shutin, and U.-C Fiebig,., "Delay-Dependent Doppler Probability Density Functions for Vehicle-to-Vehicle Scatter Channels," IEEE Trans. Ant. Propagat., in press, 2014.

[15] A. G. Zajic and G. L. Stuber, “Three-Dimensional Modeling, Simulation, and Capacity Analysis of Space–Time Correlated Mobile-to-Mobile Channels,” IEEE Trans. Veh. Technol., vol. 57, no. 4, pp. 2042-2054, Jul. 2008.

[16] A. G. Zajic, G. L. Stuber, T. G. Pratt and S. T. Nguyen, “Wideband MIMO Mobile-to-Mobile Channels: Geometry-Based Statistical Modeling with Experimental Verification,” IEEE Trans. Veh. Technol., vol. 58, no. 2, pp. 517-534, Feb. 2009.

[17] A. G. Zajic and G. L. Stuber, “Three-Dimensional Modeling and Simulation of Wideband MIMO Mobile-to-Mobile Channels,” IEEE Trans. Wirel. Commun., vol. 8, no. 3, pp. 1260-1275, Mar. 2009.

[18] A. G. Zajic, “Impact of Moving Scatterers on Vehicle-to-Vehicle Narrowband Channel Characteristics,” IEEE Trans. Veh. Technol., in press, 2014.

[19] Y. Yuan, C. X. Wang, X. Cheng, B. Ai and D. I. Laurenson, “Novel 3D Geometry-Based Stochastic Models for Non-Isotropic MIMO Vehicle-to-Vehicle Channels,” IEEE Trans. Wirel. Commun., vol. 13, no. 1, pp. 298-309, Jan. 2014.

[20] J. Karedal, F. Tufvesson, N. Czink, A. Paier, C. Dumard, T. Zemen, C. F. Mecklenbrauker and A. F. Molisch, “A Geometry-Based Stochastic MIMO Model for Vehicle-to-Vehicle Communications,” IEEE Trans. Wirel. Commun., vol. 8, no. 7, pp. 3646-3657, Jul. 2009.

[21] O. Renaudin, V.-M Kolmonen, P. Vainikainen and C. Oestges, "Wideband Measurement-Based Modeling of Inter-Vehicle Channels in the 5-GHz Band,” IEEE Trans. Veh. Technol., vol. 62, no. 8, pp. 3531-3540, Oct. 2013.

[22] L. Cheng, D. D. Stancil and F. Bai, "A Roadside Scattering Model for the Vehicle-to-Vehicle Communication Channel," IEEE Journal Select. Areas Commun., vol. 31, no. 9, pp. 449-459, Sep. 2013.

[23] G. Matz, “On Non-WSSUS Wireless Fading Channels,” IEEE Trans. Wirel. Commun., vol. 4, no. 5, pp. 2465-2478, Sep. 2005.

[24] A. Ispas, C. Schneider, G. Ascheid and R. Thoma. "Analysis of the Local Quasi-Stationarity of Measured Dual-Polarized MIMO Channels," arXiv:1401.1138, 2014.

[25] P. A. Bello, “Characterization of Randomly Time-Variant Linear Channels,” IEEE Trans. Commun., Systems, pp. 360-393, Dec. 1963.

[26] L. Bernado, T. Zemen, A. Paier, J. Karedal and B. H. Fleury, "Parametrization of the Local Scattering Function Estimator for Vehicular-to-Vehicular Channels," IEEE Veh. Technol. Conf. (VTC), Sep. 2009.

[27] L. Bernado, T. Zemen, F. Tufvesson, A. F. Molisch, and C. F. Mecklenbrauker, "Delay and Doppler Spreads of Non-Stationary Vehicular Channels for Safety Relevant Scenarios," IEEE Trans. Veh. Technol., in press, 2013.

[28] L. Bernado et al, "Non-WSSUS Vehicular Channel Characterization at 5.2 GHz-Spectral Divergence and Time-Variant Coherence Parameters," Assembly Intern. Union Radio Science (URSI), pp. 9-15, Aug. 2008.

[29] L. Bernado, T. Zemen, F. Tufvesson, A. F. Molisch, and C. F. Mecklenbrauker, "The (in-) Validity of the WSSUS Assumption in Vehicular Radio Channels," IEEE Intern. Sympos. Pers. Indoor Mobile Radio Commun. (PIMRC), pp. 1757-1762, Sep. 2012.

[30] U. A. Chude-Okonkwo, R. Ngah and T. A. Rahman, "Time-Scale Domain Characterization of non-WSSUS Wideband Channels," Springer EURASIP Journal Adv. Signal Proc., Dec. 2011.

[31] G. Acosta-Marum and M.-A. Ingram, "Six Time- and Frequency- Selective Empirical Channel Models for Vehicular Wireless LANs," IEEE Veh. Technol. Mag., vol. 2, no. 4, pp. 4-11, Dec. 2007.

[32] G. Acosta-Marum and M.-A. Ingram, "Model Development for the Wideband Expressway Vehicle-to-Vehicle 2.4 GHz Channel," IEEE Wirel. Commun. Netw. Conf., (WCNC), pp. 1283-1288, Apr. 2006.

[33] I. Sen, D. W. Matolak, "Vehicle–Vehicle Channel Models for the 5-GHz Band," IEEE Trans. Intell. Transp. Systems, vol. 9, no. 2, pp. 235-245, Jun. 2008.

[34] Y. Li, B. Ai, X. Cheng, S. Lin and Z. Zhong. A TDL Based Non-WSSUS Vehicle-to-Vehicle Channel Model," Hindawi Intern. Journal Ant. Propagat., Article ID: 103461, 2013.

[35] O. Renaudin, V. Kolmonen, P. Vainikainen and C. Oestges, "Non-Stationary Narrowband MIMO Inter-Vehicle Channel Characterization in the 5-GHz Band," IEEE Trans. Veh. Technol., vol. 59, no. 4, pp. 2007-2015, May 2010.

[36] M. Herdin, N. Czink, H. Özcelik and E. Bonek, "Correlation Matrix Distance, a Meaningful Measure for Evaluation of Non-Stationary MIMO Cannels," IEEE Veh. Technol. Conf. (VTC), Jun. 2005.

[37] Y. Jeong, J. W. Chong, H. Shin, M. Z. Win, "Intervehicle Communication: Cox-Fox Modeling," IEEE Journal Select. Areas Commun., vol. 31, no. 9, pp. 418-433, Sep. 2013.

[38] M. Boban, T. T. V. Vinhoza, M. Ferreira, J. Barros, O. K. Tonguz, "Impact of Vehicles as Obstacles in Vehicular Ad Hoc Networks," IEEE Journal Select. Areas Commun., vol. 29, no. 1, pp. 15-28, Jan. 2011.

[39] A. S. Akki and F. Haber, "A Statistical Model of Mobile-to-Mobile Land Communication Channel," IEEE Trans. Veh. Technol., vol. 35, no. 1, pp. 2-7, Feb. 1986.

[40] A. S. Akki, "Statistical Properties of Mobile-to-Mobile Land Communication Channels," IEEE Trans. Veh. Technol., vol.4 3, no. 4, pp. 826-831, Nov. 1994.

[41] F. Vatalaro and A. Forcella, “Doppler Spectrum in Mobile-to-Mobile Communications in the Presence of Three-Dimensional Multipath Scattering,” IEEE Trans. Veh. Technol., vol. 46, no. 1, pp. 213-219, Feb. 1997.

[42] P. T. Samarasinghe, T. D. Abhayapala, T. A. Lamahewa and R. A. Kennedy, "Second-order statistics of 2D non isotropic mobile-to-mobile wireless channels,” IEEE Intern. Sympos. Pers. Indoor Mobile Radio Commun. (PIMRC), pp. 1667-1671, Sep. 2011.

[43] P. T. Samarasinghe, T. A. Lamahewa, T. D. Abhayapala and R. A. Kennedy, " 3D Mobile-to-Mobile wireless channel model,” Australian Workshop Commun. Theory, pp. 30-34, 2-5 Feb. 2010.

[44] M. I. Akram and A. U. Sheikh, "Modelling and Simulation of a Generalised Vehicle-to-Vehicle Fading Channel," IET Commun., vol. 7, no. 9, pp. 818-827, Jun. 2013.

[45] M. I. Akram and A. U. Sheikh, “On the Statistical Properties of Nakagami-Hoyt Vehicle-to-Vehicle Fading Channel under Nonisotropic Scattering,” Hindawi, Intern. Journal Ant. Propagat. Article ID: 179378, 2012.

[46] J. Zhang, X. Yi and X.Cheng, "Theoretical Analysis and Measurements: Doppler Spectra of Vehicular Communication Channels," IEEE ITS Telecommun. (ITST), pp. 98-102, Nov. 2012.

[47] A. Borhani and M. Patzold, "Correlation and Spectral Properties of Vehicle-to-Vehicle Channels in the Presence of Moving Scatterers,” IEEE Trans. Veh. Technol., vol. 62, no. 9, pp. 4228-4239, Nov. 2013.

[48] F. Hlawatsch and G. Matz, (eds.) Wireless Communications over Rapidly Time-Varying Channels, Elsevier, 2011.

[49] G. D. Durgin, “Space-Time Wireless Channels,” Prentice Hall, 2003.

[50] P. Karadimas, B. Allen and P. Smith, “Human Body Shadowing Characterization for 60 GHz Indoor Short-Range Wireless Links,” IEEE Ant. Wirel. Propagat. Letters, vol. 12, pp. 1650-1653, 2013.

[51] A. F. Molisch, “Wireless Communications,” Wiley, 2005.

[52] J. Karedal, N. Czink, A. Paier, F. Tufvesson, and A. F. Molisch, “Path Loss Modeling for Vehicle-to-Vehicle Communications,” IEEE Trans. Veh. Technol., vol. 60, no. 1, pp. 323-328, Jan. 2011.

[53] G. D. Durgin, T. S. Rappaport and D. A. de Wolf, “New Analytical Models and Probability Density Functions for Fading in Wireless Communications,” IEEE Trans. Commun., vol. 50, no. 6, pp. 1005-1015, Jun. 2002.

[54] A. Abdi, “On the Utility of Laguere Series for the Envelope PDF in Multipath Fading Channels,” IEEE Trans. Inf. Theory, vol. 55, no. 12, pp. 5652-5660, Dec. 2009.

[55] A. Abdi, H. Hashemi and S. Nader-Esfahani, “On the PDF of the Sum of Random Vectors,” IEEE Trans. Commun., vol. 48, no. 1, pp. 7-12, Jan. 2000.

[56] L. Bernado, T. Zemen, F. Tufvesson, A. F. Molisch, and C. F. Mecklenbrauker, “Time-, Frequency-, and Space-varying K-Factor of Non-Stationary Vehicular Channels for Safety Relevant Scenarios,” IEEE Trans. Veh. Technol., submitted, arXiv:1306.3914, 2014.

[57] J. D Parsons and A. M. D. Turkmani, “Characterization of Mobile Radio Signals: Model Description,” IEE Proc. vol. 138, no. 6, pp. 549-556, Dec. 1991.

[58] R. Torres, B. Cobo, D. Mavares, F. Medina, S. Loredo and M. Engels, “Measurement and Statistical Analysis of the Temporal Variations of a Fixed Wireless Link at 3.5 GHz,” Springer Wirel. Pers. Commun., vol. 37, no. 1, 2, pp. 41-59, Apr. 2006.

[59] J. P. Kermoal, L. Schumacher, K. I. Pedersen, P. E. Mogensen and F. Frederiksen, "A Stochastic MIMO Radio Channel Model with Experimental Validation," IEEE Journal Select. Areas Commun., vol. 20, no. 6, pp. 1211-1226, Aug. 2002.

[60] H. Ozcelik, M. Herdin, W. Weichselberger, J. Wallace and E. Bonek, "Deficiencies of 'Kronecker' MIMO radio channel model," Electr. Letters, vol. 39, no. 16, pp. 1209-1210, Aug. 2003.

[61] W. Weichselberger, M. Herdin, H. Ozcelik and E. Bonek, “A Stochastic MIMO Channel Model with Joint Correlation of both Link Ends,” IEEE Trans. Wirel. Commun., vol. 5, no. 1, pp. 90-100, Jan. 2006.

[62] A. S. Y. Poon, D. N. C. Tse and R. W. Brodersen, "Impact of Scattering on the Capacity, Diversity, and Propagation Range of Multiple-Antenna Channels," IEEE Trans. Inf. Theory, vol. 52, no. 3, pp. 1087-1100, Mar. 2006.

[63] P. Karadimas and J. Zhang, “A Generalized Analysis of Three-Dimensional Anisotropic Scattering in Mobile Wireless Channels-Part I: Theory,” IEEE, Veh. Technol. Conf. (VTC), May 2011.

[64] P. Karadimas and J. Zhang, “A Generalized Analysis of Three-Dimensional Anisotropic Scattering in Mobile Wireless Channels-Part II: Second-Order Statistical Characterization,” IEEE, Veh. Technol. Conf. (VTC), Sep 2012.

[65] P. Karadimas, E. D. Vagenas and S. A. Kotsopoulos, “On the Scatterers’ Mobility and Second Order Statistics of Narrowband Fixed Outdoor Wireless Channels,” IEEE Trans. Wirel. Commun., vol. 9, no. 7, pp. 2119-2124, Jul. 2010.

[66] J. Jun, “Understanding the Variability of Speed Distributions under Mixed Traffic Conditions caused by Holiday Traffic,” Elsevier, Transp. Res. C, Emerging Technol., vol. 18, no. 4, pp. 599–610, Aug. 2010.

[67] C.-M. Hsu and F.-L. Lian, “A Case Study on Highway Flow Model using 2-D Gaussian Mixture Modeling,” IEEE Intell. Transp. Systems Conf. (ITSC), pp. 790–794, Sep. 2007.

[68] I. S. Gradshteyn and I. M. Ryzhik, “Tables of Integrals, Series and Products,” 7th ed., Academic Press, 2007.

[69] A. Papoulis and S. U. Pillai, “Probability, Random Variables and Stochastic Processes,” 4th ed., McGraw–Hill, 2002.

[70] J. M. Morris and J. L. Chang, “Burst Error Statistics of Simulated Viterbi Decoded BFSK and High-Rate Punctured Codes on Fading and Scintillating Channels,” IEEE Trans. Commun., vol. 43, no. 2/3/4, pp. 695–700, Feb./Mar./Apr. 1995.

[71] L. F. Chang, “Throughput Estimation of ARQ Protocols for a Rayleigh Fading Channel Using Fade- and Interfade-Duration Statistics,” IEEE Trans. Veh. Technol., vol. 40, no. 1, pp. 223–229, Feb. 1991.

[72] M. Patzold, “Mobile Fading Channels,” Wiley, 2002.